CANADIAN THESES
63921
THESES CANADIENNES

AUTHOR/AUTEUR
PIERCY, P.

PHOTODESORPTION VIA...

ISBN
0-315-16012-8

CANADIAN THESES ON MICROFICHE

I.S.B.N.

THESES CANADIENNES SUR MICROFICHE

National Library of Canada
Collections Development Branch

Canadian Theses on
Microfiche Service

Ottawa, Canada
K1A 0N4

Bibliothèque nationale du Canada
Direction du développement des collections

Service des thèses canadiennes
sur microfiche

NOTICE

The quality of this microfiche is heavily dependent upon the quality of the original thesis submitted for microfilming. Every effort has been made to ensure the highest quality of reproduction possible.

If pages are missing, contact the university which granted the degree.

Some pages may have indistinct print especially if the original pages were typed with a poor typewriter ribbon or if the university sent us a poor photocopy.

Previously copyrighted materials (journal articles, published tests, etc.) are not filmed.

Reproduction in full or in part of this film is governed by the Canadian Copyright Act, R.S.C. 1970, c. C-30. Please read the authorization forms which accompany this thesis.

THIS DISSERTATION
HAS BEEN MICROFILMED
EXACTLY AS RECEIVED

AVIS

La qualité de cette microfiche dépend grandement de la qualité de la thèse soumise au microfilmage. Nous avons tout fait pour assurer une qualité supérieure de reproduction.

S'il manque des pages, veuillez communiquer avec l'université qui a conféré le grade.

La qualité d'impression de certaines pages peut laisser à désirer, surtout si les pages originales ont été dactylographiées à l'aide d'un ruban usé ou si l'université nous a fait parvenir une photocopie de mauvaise qualité.

Les documents qui font déjà l'objet d'un droit d'auteur (articles de revue, examens publiés, etc.) ne sont pas microfilmés.

La reproduction, même partielle, de ce microfilm est soumise à la Loi canadienne sur le droit d'auteur, SRC 1970, c. C-30. Veuillez prendre connaissance des formules d'autorisation qui accompagnent cette thèse.

LA THÈSE A ÉTÉ
MICROFILMÉE TELLE QUE
NOUS L'AVONS REÇUE

NL-339 (r. 82/08)

Canada

103

0-315-16012-8

National Library of Canada | Bibliothèque nationale du Canada

Canadian Theses Division | Division des thèses canadiennes

Ottawa, Canada
K1A 0N4

63921

PERMISSION TO MICROFILM — AUTORISATION DE MICROFILMER

• Please print or type — Écrire en lettres moulées ou dactylographier

Full Name of Author — Nom complet de l'auteur

PIERCY, PETER

Date of Birth — Date de naissance

28/7/58

Country of Birth — Lieu de naissance

CANADA

Permanent Address — Résidence fixe

14 KAYMAR DR.
OTTAWA
ONTARIO
K1J 7C9

Title of Thesis — Titre de la thèse

PHOTODESORPTION VIA RESONANT LASER-MOLECULAR VIBRATIONAL COUPLING

University — Université

UNIVERSITY OF ALBERTA

Degree for which thesis was presented — Grade pour lequel cette thèse fut présentée

M.Sc.

Year this degree conferred — Année d'obtention de ce grade

1983

Name of Supervisor — Nom du directeur de thèse

Dr. H.J. KREUZER

Permission is hereby granted to the NATIONAL LIBRARY OF CANADA to microfilm this thesis and to lend or sell copies of the film.

The author reserves other publication rights, and neither the thesis nor extensive extracts from it may be printed or otherwise reproduced without the author's written permission.

L'autorisation est, par la présente, accordée à la BIBLIOTHÈQUE NATIONALE DU CANADA de microfilmer cette thèse et de prêter ou de vendre des exemplaires du film.

L'auteur se réserve les autres droits de publication; ni la thèse ni de longs extraits de celle-ci ne doivent être imprimés ou autrement reproduits sans l'autorisation écrite de l'auteur.

Date

Jan. 14/83

Signature

Peter Piercy

NL-91 (4/77)

THE UNIVERSITY OF ALBERTA

PHOTODESORPTION VIA RESONANT LASER-MOLECULAR VIBRATIONAL COUPLING

by

PETER PIERCY

A THESIS

SUBMITTED TO THE FACULTY OF GRADUATE STUDIES AND RESEARCH

IN PARTIAL FULFILLMENT OF THE REQUIREMENTS FOR THE DEGREE

OF MASTER OF SCIENCE

DEPARTMENT OF PHYSICS

EDMONTON, ALBERTA

SPRING, 1983

THE UNIVERSITY OF ALBERTA

RELEASE FORM

NAME OF AUTHOR: Peter Piercy

TITLE OF THESIS: Photodesorption via Resonant Laser-Molecular Vibrational Coupling.

DEGREE FOR WHICH THESIS WAS PRESENTED: M. Sc.

YEAR THIS DEGREE GRANTED: 1983

Permission is hereby granted to THE UNIVERSITY OF ALBERTA LIBRARY to reproduce single copies of this thesis and to lend or sell such copies for private, scholarly or scientific research purposes only.

The author reserves other publication rights, and neither the thesis nor extensive extracts from it may be printed or otherwise reproduced without the author's written permission.

(SIGNED) Peter Piercy

PERMANENT ADDRESS:

14 Kaymar Drive

Ottawa, Ontario

K1J 7C9

DATED: December 14, 1982

THE UNIVERSITY OF ALBERTA

FACULTY OF GRADUATE STUDIES AND RESEARCH

The undersigned certify that they have read, and recommend to the Faculty of Graduate Studies and Research, for acceptance, a thesis entitled "PHOTODESORPTION VIA RESONANT LASER-MOLECULAR VIBRATIONAL COUPLING" submitted by PETER PIERCY in partial fulfillment of the requirements for the degree of Master of Science.

M R ...
Supervisor

John Stephenson

Bruce L Clarke

P P Stoicheff

DATE: Dec 14, 1982

ABSTRACT

A theory of photodesorption via resonant laser excitation of internal adsorbate molecular vibrations is presented. It is applied to physisorbed molecules at low surface coverage on both dielectric and perfect conductor substrates.

Effects of the laser, phonons, and tunneling are included in a calculation of microscopic transition rates among the states of the physisorption surface bond. Derivation of the macroscopic desorption rate is achieved by numerical solution of a master rate equation incorporating the microscopic phenomena. Desorption is found to be both temperature and laser intensity dependent, from low temperatures up to the thermal desorption regime, and for intensities up to saturation. The influence of the system parameters - including the molecular vibrational frequency and the depth and range of the physisorption potential- on desorption is also elucidated. Finally, results presented for the CH_3F/NaCl and CO/Cu systems are compared with experiments in the literature.

ACKNOWLEDGEMENTS

The project described in this thesis would have certainly been inconceivable without the most necessary direction and assistance of Drs. H.J. Kreuzer and Z.W. Gortel. Specifically, Dr. Kreuzer is thanked for providing me with both "the problem" and the theoretical machinery with which to tackle it, and for his suggestions after reading the entire thesis draft. Dr. Gortel's instruction, and his calculation notes which form the basis of this work, I gratefully acknowledge. The final analysis became a joint effort; this thesis is as much a culmination of their work as of mine.

The numerical computations were done by R. Teshima, whose expert work is very much appreciated.

TABLE OF CONTENTS

		Page
1.	INTRODUCTION	1
2.	CALCULATION OF THE PHOTODESORPTION RATES	6
	2.1 Summary of Program	6
	2.2 Quantization of the Laser Radiation	10
	2.3 Hamiltonian of the Gas-Solid-Laser System	17
	2.3.1 The static Hamiltonian	18
	2.3.2 The electromagnetic field interaction	21
	2.3.3 Dynamics of the solid - phonons	22
	2.3.4 The complete Hamiltonian	24
	2.4 Calculation of the Transition Rates	25
	2.4.1 Application of the perturbation theory	25
	2.4.2 $\vec{Y}(j,v,j',v')$ and $L_{jj'}^{vv'}$	27
	2.4.3 The phonon interaction; $\vec{X}$ and $P_{jj'}^{vv'}$	33
	2.4.4 The tunneling transition; $Q_{cj'}^{vv'}$	38
	2.5 Solution of the Master Equation	40
3.	NUMERICAL RESULTS AND DISCUSSION	42
	3.1 Characterization of our Photodesorption Model	42
	3.2 Comparison with Early Experiments; Discussion	59
	3.3 Other Theories	63
4.	CONCLUSIONS	67
	REFERENCES	69

TABLE OF CONTENTS (cont'd)

		Page
Appendix A	- Orthogonality of $\{\vec{U}_{\vec{k}\beta}\}$	71
Appendix B	- The Morse Wave Functions	73
Appendix C	- Evaluation of the Integral $I_{\ell jj'}$	75

LIST OF TABLES

Table		Page
1.	System parameters for CH_3F on NaCl.	43
2.	Desorption rates for the CH_3F/NaCl systems.	58

LIST OF FIGURES

Figure		Page
1.	Possible channels to desorption.	3
2.	The interaction process.	6
3a.	Energy diagram of gas molecule states.	7
3b.	Two possible paths to desorption.	7
4a.	The semi-infinite solid.	10
4b.	Ray diagram of laser radiation.	12
5.	Adsorbate molecule configuration.	18
6.	Angular dependence of the vibrational transition rate.	32
7.	Energy levels for the CH_3F/NaCl systems.	45
8.	Log rate versus log fluence for system A.	46
9.	Log rate versus inverse temperature for system A.	47
10.	Log rate versus log fluence for system B.	49
11.	Log rate versus inverse temperature for system B.	50
12.	Typical transition rates occurring in system B.	52
13.	Path to desorption at high temperatures.	54
14.	Log rate versus log fluence for system C.	56
15.	Log rate versus inverse temperature for system C.	57
16.	A laser-induced heating mechanism.	62
17.	Log rate versus log fluence for the CO/Cu system.	65
18.	Desorption mechanism for the H_2/Al_2O_3 system.	66

§1. INTRODUCTION

The kinetics of gas-solid surface interactions has been a subject of escalating interest - both experimental and theoretical - in recent years. Chemical reactions catalyzed at solid surfaces are of fundamental importance - to industrial applications, for example - and their kinetic theory is under current development. The processes of adsorption and desorption of gas molecules at a solid surface are an important part of complex catalytic reactions.

Adsorption is the process whereby gas phase particles enter into an energetically favourable configuration at a solid surface. (Desorption occurs when gas particles leave this configuration.) If the bond formed between the gas and surface molecules is strong, with binding energy typically greater than 1 eV, then the reaction is called chemisorption. In this case extensive "electron sharing" occurs between gas and solid atoms. While this reaction is of prime importance to catalysis, we consider instead the weaker gas-surface interaction of physisorption. A gas molecule is said to be physisorbed at a surface if the bond is weak - typically with binding energy <1 eV. In this case electron sharing is minimal, and the gas molecules are chemically unaltered after undergoing an adsorption and desorption process. We will focus our attention on the desorption of physisorbed polyatomic molecules.

Desorption may proceed via many different channels; two of major current interest are summarized below:

i) The thermal motion of the solid surface may couple to the gas-solid bond. See Fig. 1a. By absorption of phonons, the surface bond may be excited to a continuum state, in which case desorption occurs. This process, called thermal desorption, has been analyzed, using a full quantum statistical theory, by Gortel and Kreuzer[1,2]. Two common methods for initiating the reaction are 1) reducing the gas pressure at the surface, and 2) heating the solid either slowly ("programmed thermal desorption") or rapidly ("flash desorption").

Experiments show that the single gas particle desorption rate may, in a certain regime, be parameterized by an Arrhenius-type formula[3]:

$$t_d^{-1} = \nu\, e^{-E_d/kT} \qquad (1)$$

where t_d is the characteristic desorption time, T is the solid temperature, E_d is the heat of adsorption, and ν is a prefactor that is classically approximated by the vibrational frequency of the particle in the surface bond. The more general theory of Gortel and Kreuzer[1] predicts desorption via a cascade of step by step phonon-assisted transitions up through the surface bond states into the continuum. Their results, which agree well with experiments, also delineate the regime in which the simple formula given above may be applied.

ii) Another means of stimulating desorption is to irradiate the surface with high intensity laser light - hence photodesorption. The radiation energy may couple to the adsorbate-solid system either 1) by directly heating the solid via non-resonant absorption of radiation from a large laser pulse[4], 2) by direct excitation of the adsorbate-surface bond[5,6], or 3) by resonant excitation of an internal vibrational mode of an adsorbate molecule[7-10]. (See Figs. 1b,c,d, respectively.)

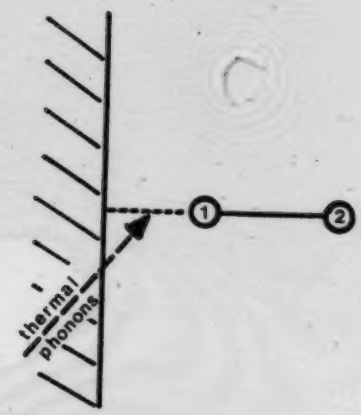

a) thermal desorption

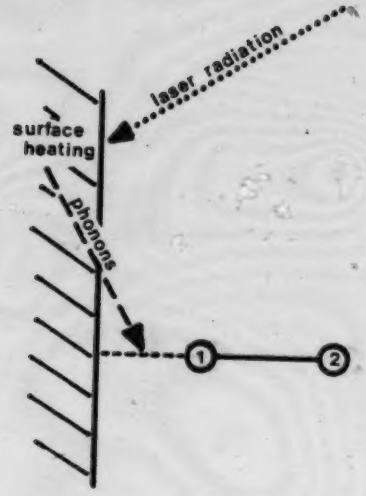

b) laser-induced
thermal desorption

c) laser excites
surface bond directly

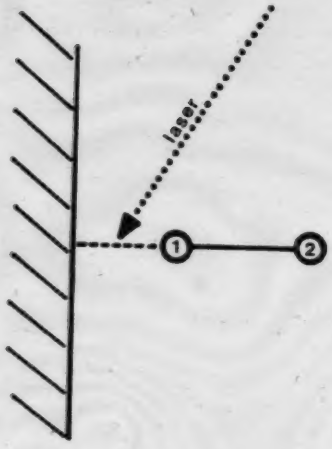

d) laser excites
molecular vibrations

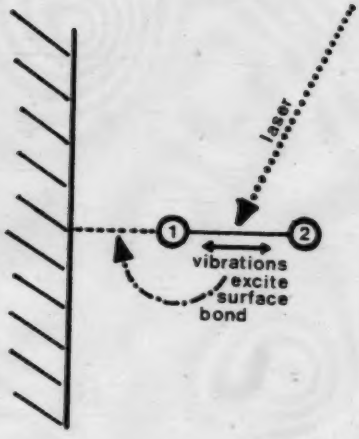

Fig. 1. Possible channels to desorption.

We will only consider systems at low surface coverage, and have therefore ignored the possibility of interactions between the adsorbate molecules themselves.

Reaction mechanism (1) above proceeds via thermal desorption from a suddenly heated surface, and has been termed "laser flash desorption". On the other hand, the surface bond itself absorbs the laser radiation in channel (2). Finally, reaction channel (3) permits the resonant absorption of light by the adsorbate molecule itself, with subsequent tunneling processes leading to desorption. It is anticipated that mechanism (3) will generally be more efficient than (2), because anharmonicity of the surface potential makes light absorption in (2) largely non-resonant. This is explained in greater detail in Section 3.3.

We concentrate on channel (3) above. Since different species of adsorbate molecules have different radiation absorption spectra, mechanism (3) may possibly be used to selectively excite the particular species we wish to desorb, by tuning the laser frequency appropriately. The possibility then exists of using this mechanism to purify and separate substances, or to determine the individual molecular populations of a multicomponent adsorbate.

Some basic details of the gas-solid system that we consider are now presented. It is reminded that we deal only with a physisorbed, low coverage adsorbate at very low gas pressures. We assume further that the adsorbate molecules reside at localized sites and are not free to move laterally on the surface. The solid is treated as a continuum, which interacts with the adsorbate via its surface only. Our adsorbate consists of diatomic molecules adsorbed end on - that is, with one atom much closer to the surface than the other. We may model

some polyatomic molecules too, by replacing the outer "atom" above with a complex (e.g. $F-CH_3$). The rotational motion of gas molecules, whether adsorbed or free, is ignored. By ignoring surface heating effects via channel (1) above, the choice of solid is restricted to either a dielectric which is transparent at laser frequencies, or to a very good conductor. (In the latter case we must also be careful to not use too high laser intensities[8b].) Finally, our model process for resonant photodesorption requires a laser that can be tuned to the infrared spectral line of the appropriate vibrational mode of an adsorbate molecule.

Within the bounds of this model, we will calculate, in a quantum mechanical formalism, microscopic transition rates from which the macroscopic desorption phenomena can be derived; see Section 2. The phenomenological characteristics of our model are studied in Section 3, where a comparison is made with presently available experimental results and with other theories in the literature. Concluding remarks are found in Section 4.

§2. CALCULATION OF THE PHOTODESORPTION RATES

§2.1 Summary of Program

We want to treat the interaction process of Fig. 2 quantum mechanically, and develop rate equations to describe the desorption process.

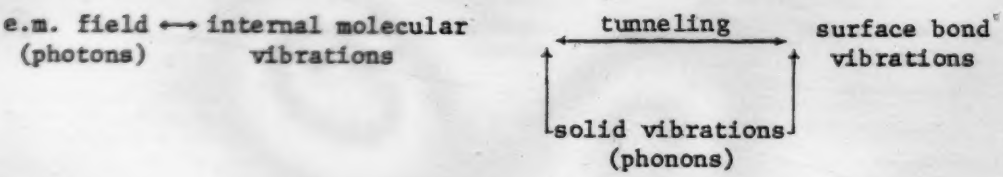

Fig. 2. The interaction process.

Suppose the surface bond is described by a potential well (see Fig. 3a) which has bound (adsorbed) states labelled by the quantum number j, and a continuum of free states, each denoted q. (We will use a Morse potential to model the surface bond.) Further, assume that internal vibrations of the adsorbed gas molecule are approximately simple harmonic, giving an energy spectrum of equally spaced levels denoted by the vibrational state index v. The double-index (j,v) fully describes the state of an adsorbate molecule in our theory. The interaction process in Fig. 2 causes transitions between the states (j,v). If a gas molecule, previously adsorbed in the state (j',v'), is transferred to a free state (q,v), then the surface bond is broken and the molecule leaves the surface with some translational velocity. This process is called desorption. Note that an adsorbate molecule in state (j,v) may have total energy greater than zero, if the positive contribution due to the internal vibrational state (v) exceeds the negative portion due to the bound surface state (j). Whether the molecule is adsorbed or free depends on the surface bond index (j or q) only. As

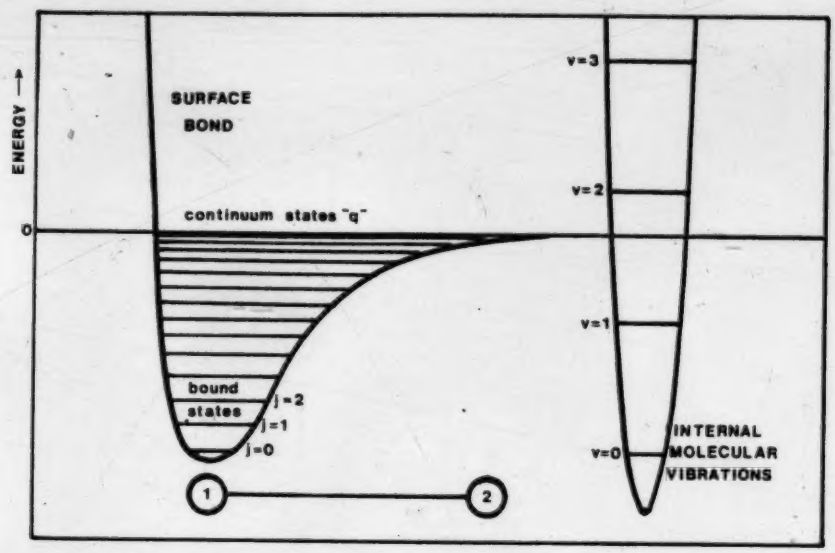

Fig. 3a. Energy diagram of gas molecule states.

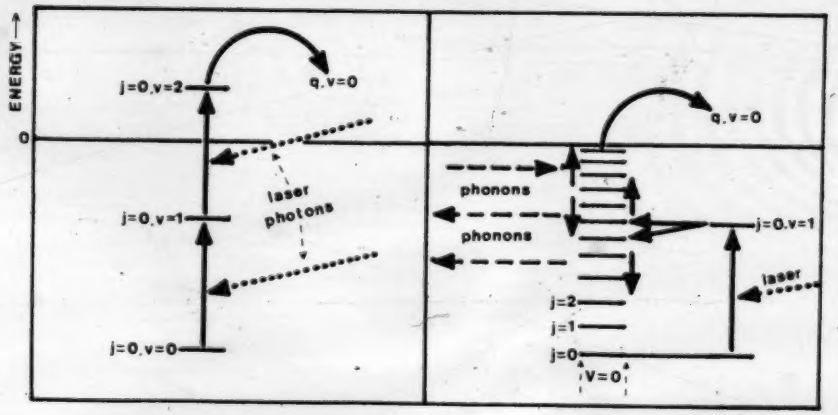

Fig. 3b. Two possible paths to desorption.

an example, two possible transition paths to desorption are shown graphically in Fig. 3b. Notice that the path to desorption may be very complex, involving many transitions along the way.

We assume that the dynamics of the adsorbate molecules is a stationary Markov process. Defining the state occupation numbers $n_j^v(t)$ we describe the time-evolution of our system by the master equation

$$\frac{d}{dt} n_j^v(t) = \sum_{(v',j')\neq(v,j)} R_{jj'}^{vv'} n_{j'}^{v'}(t) - \left(\sum_{(v',j')\neq(v,j)} R_{j'j}^{v'v} + \sum_{v'\neq v} R_{cj}^{v'v} \right) n_j^v(t) \quad . \tag{2}$$

where $R_{jj'}^{vv'}$ is the single particle transition rate from (j',v') to (j,v), $R_{cj'}^{vv'}$ is the single particle transition rate from (j',v') to all continuum states (q) with vibrational index v. ($R_{jj'}^{vv'}$ and $R_{cj'}^{vv'}$ are given by our microscopic quantum mechanical theory described later in this section.)

We assume that, initially, the adsorbate is already present on the surface and that no further adsorption occurs during the desorption process. That is, there are no transitions $(q,v') \rightarrow (j,v)$. This is reasonable since photodesorption experiments are normally performed in ultra high vacuum conditions; there are exceedingly few free gas molecules available for adsorption.

In postulating the rate equations (2), we assume that the thermal equilibrium in the solid and the steady state conditions of the laser are maintained throughout the desorption process. The role of equations (2) in a full quantum statistical formalism is elucidated in reference 1.

The desorption rate is now just the rate of depopulation of the bound states (j), and hence:

$$\text{Des.rate} = N t_d^{-1} = -\frac{d}{dt} \sum_{(j,v)} n_j^v(t) = -\sum_{(j,v)} \dot{n}_j^v(t) \qquad (3)$$

where t_d is the characteristic desorption time and $N = \sum_{(j,v)} n_j^v(0)$.

In principle, the desorption rate may be determined by solving the coupled system of rate equations (2) for specified initial conditions. We rewrite (2) in more compact form as

$$\dot{\vec{n}}(t) = \overleftrightarrow{R}\,\vec{n}(t) \qquad (4)$$

where $\vec{n}(t)$ is a column vector of occupation numbers $n_j^v(t)$ and $\overleftrightarrow{R}$ is the rate matrix, with element

$$R_{jv,j'v'} = \begin{cases} R_{jj'}^{vv'} & \text{for } (j,v) \neq (j',v') \\ -\sum_{(v'',j'')} R_{j''j}^{v''v} - \sum_{v''} R_{cj}^{v''v} & \text{for diagonal elements} \end{cases}$$

(We include only bound states (j) in the rate equations since we ignore the possibility of transitions returning from the continuum.)
Solving (4) involves a complex numerical calculation, but we may estimate the desorption time by studying the eigenvalues of matrix $\overleftrightarrow{R}$, as described in Section 2.5.[1]

It remains to calculate the transition rates $R_{jj'}^{vv'}$ and $R_{cj'}^{vv'}$ using the interaction channel described in Fig. 2. To include the laser radiation correctly, we must first determine the electromagnetic field near the solid surface in a suitable quantized form; see Section 2.2. The Hamiltonian of the gas-solid-laser system, including appropriate interaction terms, is constructed in Section 2.3. A straightforward application of time-dependent perturbation theory then gives the transition rates in Section 2.4.

§2.2 Quantization of the Laser Radiation

a) Introduction

We shall calculate the quantized electromagnetic field for the special case in which the solid is a lossless non-magnetic dielectric, and then at the end show how one can solve the problem if the solid were a perfect conductor instead.*

Suppose the dielectric filling the half space $x < 0$ is described by a uniform, scalar permitivity ε, and the $x > 0$ region is the vacuum. (See Fig. 4a). We ignore the effect of gas molecules on the electromagnetic field, since the molecular density has already been assumed to be small, both on the solid surface, and in the free gaseous state.

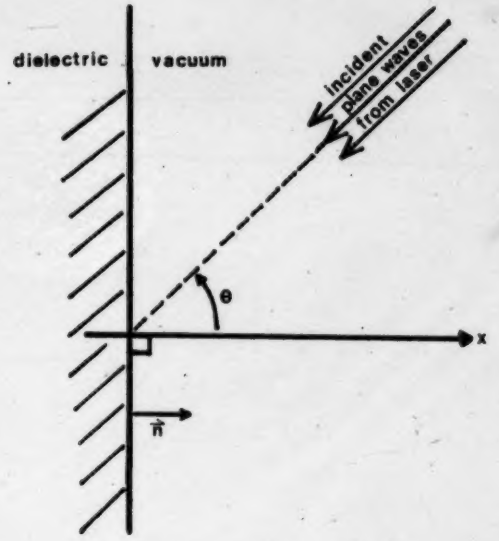

Fig. 4a. The semi-infinite solid.

---

*We can, in fact, obtain the perfect conductor results from those for the dielectric case by letting the refractive index (n_r) become infinite.

To determine the electromagnetic field near the solid surface, one solves Maxwell's equations for the appropriate geometry and boundary conditions. These equations are:

$$\nabla\cdot\vec{E}=0, \quad \nabla\cdot\vec{B}=0, \quad \nabla\times\vec{E}=-\frac{\partial\vec{B}}{\partial t}, \quad \nabla\times\vec{B}=n^2(x)\,\varepsilon_o\mu_o\,\frac{\partial\vec{E}}{\partial t} \tag{5a}$$

with

$$\vec{E}\times\vec{n}, \quad n^2(x)\,\vec{E}\cdot\vec{n}, \quad \vec{B} \text{ continuous at } x = 0 \tag{5b}$$

where

$$n(x) = \begin{cases} 1 & ; \quad x>0 \\ n_r & ; \quad x<0 \end{cases} \quad ; \; n_r=\sqrt{\frac{\varepsilon}{\varepsilon_o}} \text{ is the refractive index of the dielectric.}$$

The solutions to (5) must be consistent with incident plane waves from the $x>0$ side. Combining (5a) gives the wave equations

$$\nabla^2 u - \frac{1}{v^2(x)}\frac{\partial^2 u}{\partial t^2} = 0 \tag{6}$$

where u is a component of $\vec{E}$ or $\vec{B}$, and $v(x) = \frac{c}{n(x)}$ is identified as the wave velocity.

Introducing the vector potential, $\vec{A}(\vec{x},t)$, in the Coulomb gauge in the usual manner, we have

$$\vec{E} = -\frac{\partial\vec{A}}{\partial t}, \quad \vec{B} = \nabla\times\vec{A}, \quad \nabla\cdot\vec{A} = 0 . \tag{7}$$

Substituting (7) into (5a,b), the problem is rewritten as

$$\nabla^2\vec{A} - \frac{1}{v^2(x)}\frac{\partial^2\vec{A}}{\partial t^2} = 0 \tag{8a}$$

where

$$\vec{n}\times\vec{A}, \quad \nabla\times\vec{A}, \quad n^2(x)\,\vec{A}\cdot\vec{n} \text{ are continuous at } x = 0 . \tag{8b}$$

For the quantization procedure (described formally in (c)) we will need to expand the electromagnetic potential $\vec{A}(\vec{x},t)$ in terms of a set of orthogonal modes $\{\vec{U}_{k\beta}(\vec{x})\}$ which independently satisfy equations (8):

$$\vec{A}(\vec{x},t) = \sum_{\vec{k},\beta} \left(\phi_{\vec{k}\beta}\, \vec{U}_{\vec{k}\beta}(x)\, e^{-i\Omega_{\vec{k}\beta} t}\, C_{\vec{k}\beta} + \text{hermitian conjugate} \right) \qquad (9)^*$$

where $\vec{k}$ and β are the incident wave vector and polarization of the mode, $\phi_{\vec{k}\beta}$ is a normalization constant, $C_{\vec{k}\beta}$ is the mode amplitude, that will become the annihilation operator after quantization and $\Omega_{\vec{k}\beta}$ is the oscillation frequency.

In Section (b) we construct a suitable set of modes $\{\vec{U}_{\vec{k}\beta}(\vec{x})\}$ and present the appropriate orthogonality relations needed in the quantization formalism described in Section (c).

b) Orthogonal modes

To find solutions of equations (8) appropriate to the laser radiation, we consider a plane wave incident on the dielectric at angle θ, as shown in Fig. 4b. Instead of solving (8) directly, we determine the

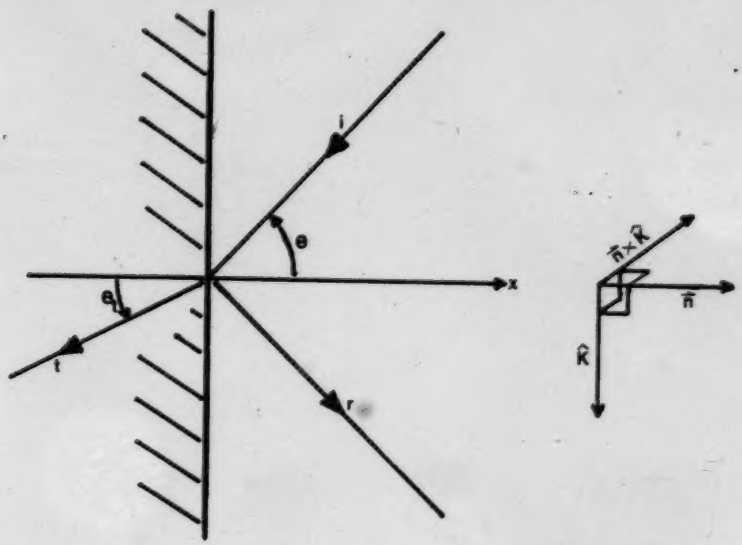

Fig. 4b. Ray diagram of laser radiation.

*The sum in equation (9) is symbolic for $\sum_{\beta}\int d\vec{k}$. Since the system is of infinite size, the mode wave number ($\vec{k}$) is continuous.

reflected and transmitted waves using Snell's law and Fresnel's equations[11]. The wave vectors of the incident, reflected and transmitted waves are respectively:

$$\vec{k}_i = K\hat{K} + \zeta\vec{n}\ , \quad \vec{k}_r = \hat{K}K - \zeta\vec{n}\ , \quad \vec{k}_t = \hat{K}K - b\vec{n} \tag{10}$$

where $\zeta < 0$; $\hat{K},\vec{n}$ are shown in Fig. 4b, and $b = n_r|\vec{k}_i|\cos\theta_t = \sqrt{(n_r-1)K^2 + n_r^2\zeta^2}$ by Snell's law. We use the coordinate system $\vec{x} = \vec{R} + \vec{n}x$ where $\vec{R}\cdot\vec{n} = 0$. Let the incident radiation be described by $(\vec{A}_o^s + \vec{A}_o^p) \times e^{(i\vec{k}_i\vec{x} - \Omega t)}$, where $\Omega = c|\vec{k}_i|$ and $\vec{A}_o^\beta$ is the amplitude in the polarization β. ($\beta = s(p)$ refers to electric vector polarization perpendicular (parallel) to the plane of incidence.) Then, using Fresnel's equations to give the amplitudes of the reflected and transmitted waves, we write the total electromagnetic potential as a sum of incident, reflected, and transmitted waves as

$$\vec{A}(\vec{x},t) = [\vec{A}^s(\vec{x}) + \vec{A}^p(\vec{x})]\, e^{-i\Omega t} \tag{11}$$

where

$$\vec{A}^s(\vec{x}) = \begin{cases} \vec{A}_o^s\, e^{i\vec{K}\vec{R}}\left(e^{i\zeta x} + \dfrac{1 - n_r a}{1 + n_r a}\, e^{-i\zeta x}\right)\vec{n}\times\hat{K} & ;\ x > 0 \\ \vec{A}_o^s\, \dfrac{2}{1 + n_r a}\, e^{i\vec{K}\vec{R}}\, e^{-ibx}\, \vec{n}\times\hat{K} & ;\ x < 0 \end{cases} \tag{12}$$

$$\vec{A}^p(x) = \begin{cases} \vec{A}_o^p e^{i\vec{K}\vec{R}}\left[K\vec{n}\left(e^{i\zeta x} + \dfrac{n_r - a}{n_r + a}\, e^{-i\zeta x}\right) - \zeta\hat{K}\left(e^{i\zeta x} - \dfrac{n_r - a}{n_r + a}\, e^{-i\zeta x}\right)\right] ;\ x > 0 \\ \vec{A}_o^p\, \dfrac{2}{n_r(n_r + a)}\, e^{i\vec{K}\vec{R}}\, e^{-ibx}\,(K\vec{n} + b\hat{K}) \ ; \qquad x < 0 \end{cases}$$

with $a = \dfrac{\cos\theta_t}{\cos\theta} = -\dfrac{1}{\zeta}\sqrt{K^2(1 - 1/n_r^2) + \zeta^2}$.

$\vec{A}(\vec{x},t)$, as defined in (11) and (12), is a solution of Maxwell's equations (8).

Instead of the potential $\vec{A}^{\beta}(\vec{x})$, one requires, for quantization, a set of orthonormal modes. Define a prospective set of modes as

$$\vec{U}_{\vec{k}\beta}(\vec{x}) = \frac{1}{2\pi} e^{i\vec{K}\vec{R}} \vec{f}^{\beta}_{\vec{K}\zeta}(\vec{x}) \tag{13a}$$

where

$$\vec{f}^{s}_{\vec{K}\zeta}(\vec{R},x) = N^{s}\vec{n}\times\hat{K}\begin{cases}(e^{i\zeta x} + \frac{1-n_r a}{1+n_r a} e^{-i\zeta x}) \; ; & x>0 \\ \frac{2}{1+n_r a} e^{-ibx} \; ; & x<0\end{cases} \tag{13b}$$

$$\vec{f}^{p}_{\vec{K}\zeta}(\vec{R},x) = N^{p}\begin{cases}K\vec{n}(e^{i\zeta x}+\frac{n_r-a}{n_r+a} e^{-i\zeta x}) - \zeta\hat{K}(e^{i\zeta x}-\frac{n_r-a}{n_r+a} e^{-i\zeta x}) \; ; & x>0 \\ \frac{2}{n_r(n_r+a)} (K\vec{n}+b\hat{K}) e^{-ibx} \; ; & x<0\end{cases}$$

(N^s and N^p are normalization constants.)

The set $\{\vec{U}_{\vec{k}\beta}(\vec{x})\}$ is a suitable basis in which to expand the electromagnetic field resulting from an external radiation source on the vacuum side. As shown in Appendix A, this set obeys the orthogonality relation

$$\int d\vec{x}\, n^2(x)\, \vec{U}_{\vec{k}\beta}(\vec{x})\, \vec{U}^{*}_{\vec{k}'\beta'}(\vec{x}) = \delta_{\beta\beta'}\, \delta(\vec{k}-\vec{k}') \; . \tag{14}$$

The modes $\{\vec{U}_{\vec{k}\beta}(\vec{x})\}$ are orthogonal with respect to the weighting factor $n^2(x)$ defined in (5b). In Section (c) we find that this form of orthogonality relation is crucial in determining the form of the Hamiltonian and the commutation relations for the operator $C_{\vec{k}\beta}$.

We shall also use in (c) the additional relation:

$$\int d\vec{x}\, n^2(x) \vec{U}_{\vec{k}\beta}(\vec{x}) \cdot \vec{U}_{\vec{k}'\beta'}(\vec{x}) = -\Lambda_{\vec{k}\beta}\, \delta(\vec{K}+\vec{K}')\delta(\zeta-\zeta') \tag{15}$$

This relation is derived in Appendix A, where the coefficient $A_{\vec{k}\beta}$ is defined.

c) The quantization formalism

To quantize the electromagnetic field, we shall follow the Lagrangian formalism, as described, for example, in Haken[12]. We must first find a suitable Lagrangian that is consistent with the desired equations of motion and Hamiltonian. Since the electromagnetic fields ($\vec{E}$ and $\vec{B}$) are derived from the potential ($\vec{A}$), we will find the Lagrangian (L) to be a functional of the coordinate $\vec{A}(\vec{x},t)$ and its derivatives. The equations of motion are then

$$\frac{d}{dt}\frac{\delta L}{\delta \dot{A}_i(\vec{x},t)} - \frac{\delta L}{\delta A_i(\vec{x},t)} = 0 \qquad (16)$$

where $A_i(\vec{x},t)$ is a Cartesian component of $\vec{A}(\vec{x},t)$ and the dot means $\partial/\partial t$. Equation (16) must be consistent with the wave equation (8a) that was previously derived from Maxwell's equations. This is so if the Lagrangian is chosen to be

$$L = \frac{1}{8\pi}\int d\vec{x}'\,\frac{1}{v^2(x')}\sum_{i=1}^{3}\left[(\dot{A}_i(\vec{x}'))^2 - (\nabla A_i(\vec{x}))^2\right] . \qquad (17)$$

The constant of proportionality in the above expression was fixed by requiring that the Hamiltonian be consistent with the classical field energy expression[12]

$$H = \frac{1}{2}\int d\vec{x}\,(\varepsilon \vec{E}^2(\vec{x}) + \frac{1}{\mu}\vec{B}^2(\vec{x})) . \qquad (18)$$

Using the chosen Lagrangian (17), one may define the canonical momentum, conjugate to the coordinate $A_i(\vec{x})$ as

$$\Pi_i(\vec{x},t) \equiv \frac{\delta L}{\delta \dot{A}_i(\vec{x},t)} = \varepsilon_o n^2(x)\,\dot{A}_i(\vec{x},t) . \qquad (19)$$

Now, one makes the quantization postulate, namely that

$$[A_i(\vec{x}'),\Pi_j(\vec{x})] = i\hbar\delta^{tr}_{ij}(\vec{x}-\vec{x}') \tag{20}$$

where

$$\delta^{tr}_{ij}(\vec{x}-\vec{x}') = \delta_{ij}\delta(\vec{x}-\vec{x}') + \frac{1}{4\pi}\frac{\partial^2}{\partial x_i \partial x_j}\frac{1}{|\vec{x}-\vec{x}'|} \quad . \tag{21}$$

The first term in (21) is just the usual delta function, while the second term is included so that the commutator (20) is consistent with the gauge condition, $\nabla\cdot\vec{A} = 0$.[12]

The commutator (20) for the field coordinates, combined with the expansion for $\vec{A}(\vec{x},t)$ given in (9) and the orthogonality relations (14) and (15), together imply the commutation relations for $C_{\vec{k}\beta}$ and $C^{\dagger}_{\vec{k}'\beta'}$ given below:

$$[C_{\vec{k}\beta},\ C^{\dagger}_{\vec{k}'\beta'}] = \delta_{\beta\beta'}\delta(\vec{k}-\vec{k}') \tag{22a}$$

$$[C_{\vec{k}\beta},\ C_{\vec{k}'\beta'}] = 0 = [C^{\dagger}_{\vec{k}\beta},\ C^{\dagger}_{\vec{k}'\beta'}] \quad . \tag{22b}$$

In fact, the commutators for $C_{\vec{k}\beta}$ are given by equations (22a,b) only if $A_i(\vec{x})$ and $\Pi_j(\vec{x})$ obey equation (20).[13]

One may then express the Hamiltonian in the form

$$H = \sum_{\beta}\int d\vec{k}\,\hbar\Omega_{\vec{k}\beta}\,(C^{\dagger}_{\vec{k}\beta}C_{\vec{k}\beta} + \frac{1}{2}) \tag{23}$$

where $\Omega_{\vec{k}\beta} = c|\vec{k}|$. To derive (23), substitute the expansion (9) for $\vec{A}$ into the expression for H given in (18). Then, using the orthogonality relations (14) and (15), and the commutators (22a,b), the given result is obtained.

Interpreting $C_{\vec{k}\beta}$ and $C^{\dagger}_{\vec{k}\beta}$ as the annihilation and creation operators, respectively, of the photon states $(\vec{k},\beta)$ of the electromagnetic field,

the quantization procedure is almost complete. Formally, one must further check that the chosen set of modes $\{\vec{U}_{k\beta}(\vec{x})\}$ is complete. This is required for the theory to be self-consistent. We have not, however, performed this calculation.

d) Perfect conducting solid

If the solid is a perfect conductor (infinite conductivity) instead of a dielectric (zero conductivity), then one may perform the same quantization procedure, provided one uses instead the orthonormal modes

$$\vec{U}_{ks}(\vec{x}) = N^s e^{i\vec{K}\vec{R}}(e^{i\zeta x} - e^{-i\zeta x})\,\vec{n}\times\vec{K} \quad ; \quad x>0$$

$$\vec{U}_{kp}(\vec{x}) = N^p e^{i\vec{K}\vec{R}}\left[K\vec{n}(e^{i\zeta x}+e^{-i\zeta x}) - \zeta\hat{K}(e^{i\zeta x}-e^{-i\zeta x})\right] ; \quad x>0 \qquad (24)$$

$$\vec{U}_{ks}(\vec{x}) = \vec{U}_{kp}(\vec{x}) = 0 ; \qquad x<0$$

with

$$\int d\vec{x}\,\vec{U}_{k\beta}(\vec{x})\vec{U}^*_{k'\beta'}(\vec{x}) = \delta_{\beta\beta'}\delta(\vec{k}-\vec{k}')$$

$$\int d\vec{x}\,\vec{U}_{k\beta}(\vec{x})\vec{U}_{k'\beta'}(\vec{x}) = \delta_{\beta\beta'}\delta(\vec{K}+\vec{K}')\delta(\zeta-\zeta') \quad . \qquad (25)$$

The quantization done in Section 2.2c then carries through identically for this set of modes.

§2.3 Hamiltonian of the Gas-Solid-Laser System

We shall now construct the Hamiltonian for the gas-solid-laser system in second quantized form. We assume that the density of gas molecules is small, both on the solid surface and in the gas phase, so that gas molecule-gas molecule interactions can be neglected. The gas molecules may then be treated independently.

§2.3.1 The static Hamiltonian

We study one diatomic molecule in a vacuum near a semi-infinite static solid surface, and will ignore thermal vibrations and the electromagnetic field for now. See Fig. 5. Atoms one and two of the molecule are separated by the displacement $\vec{\xi} = \vec{x}_2 - \vec{x}_1$.

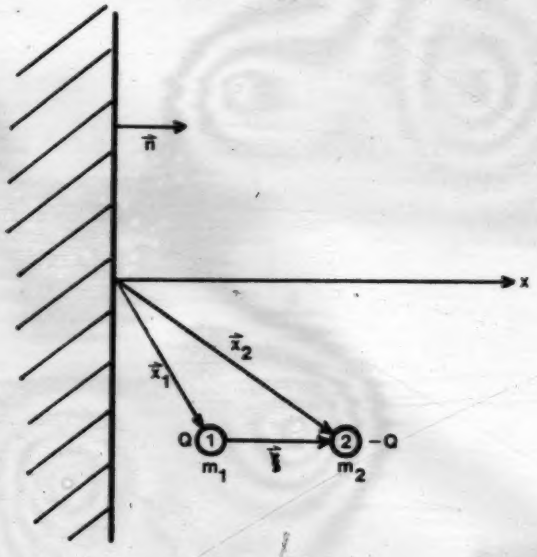

Fig. 5. Adsorbate molecule configuration.

Now let $U(\vec{\xi})$ be the interatomic potential of the molecule, and $V_i(\vec{x}_i)$ be the potential energy of the i^{th} gas atom-solid interaction ($i = 1,2$). The quantum mechanical Hamiltonian for the diatomic gas molecule and the static solid is

$$H_{st} = -\frac{\hbar^2}{2m_1}\frac{\partial^2}{\partial \vec{x}_1^2} - \frac{\hbar^2}{2m_2}\frac{\partial^2}{\partial \vec{x}_2^2} + U(\vec{\xi}) + V_1(\vec{x}_1) + V_2(\vec{x}_2) \ . \qquad (27)$$

Introducing centre of mass coordinates, H_{st} becomes

$$H_{st} = -\frac{\hbar^2}{2m}\frac{\partial^2}{\partial \vec{x}^2} - \frac{\hbar^2}{2\mu}\frac{\partial^2}{\partial \vec{\xi}^2} + U(\vec{\xi}) + V_1(\vec{x} - \frac{\mu}{m_1}\vec{\xi}) + V_2(\vec{x} + \frac{\mu}{m_2}\vec{\xi}) \qquad (28)$$

where

$$m = m_1 + m_2 ,$$

$$\mu = (m_1^{-1} + m_2^{-1})^{-1} ,$$

$$\vec{x} = \frac{1}{m}(m_1\vec{x}_1 + m_2\vec{x}_2) ,$$

$$\vec{\xi} = \vec{x}_2 - \vec{x}_1 .$$

To simplify calculations considerably, we choose to ignore the interaction between atom 2 and the solid, and thus set $V_2(\vec{x} + \frac{\mu}{m_2}\vec{\xi}) = 0$. Atom 2 is sufficiently distant from the surface to render its interaction with the solid insignificant. Then, defining

$$H_\mu(\vec{\xi}) = -\frac{\hbar^2}{2\mu}\frac{\partial^2}{\partial \vec{\xi}^2} + U(\vec{\xi})$$

$$H_m(\vec{x}) = -\frac{\hbar^2}{2m}\frac{\partial^2}{\partial \vec{x}^2} + V_1(\vec{x} - \frac{\mu}{m_1}\vec{\xi}_o) \qquad (29)$$

and

$$H_{res}(\vec{x},\vec{\xi}) = V_1(\vec{x} - \frac{\mu}{m_1}\vec{\xi}) - V_1(\vec{x} - \frac{\mu}{m_1}\vec{\xi}_o)$$

where $\vec{\xi}_o$ is the mean interatomic spacing of atoms 1 and 2, one has

$$H_{st}(\vec{x},\vec{\xi}) = H_\mu(\vec{\xi}) + H_m(\vec{x}) + H_{res}(\vec{x},\vec{\xi}) . \qquad (30)$$

Now, since $|\vec{\xi} - \vec{\xi}_o| << |\vec{\xi}_o|$ and $V_1(\vec{x})$ is a smooth function, the residual term (H_{res}) in the Hamiltonian will be small; H_{res} is therefore treated as a perturbation.

It is desirable now to find a diagonal basis for the operator $H_\mu(\vec{\xi}) + H_m(\vec{x})$. H_μ and H_m can be diagonalized independently, as expressed by equations (31a) and (31b).

$$H_\mu(\vec{\xi})u_v(\vec{\xi}) = \Delta_v u_v(\vec{\xi}) \tag{31a}$$

$$H_m(\vec{x})\phi_j(\vec{x}) = \varepsilon_j \phi_j(\vec{x}) \tag{31b}$$

where $u_v(\vec{\xi})$ is an eigenvector of H_μ with corresponding eigenvalue Δ_v and $\phi_j(\vec{x})$ is an eigenvector of H_m with corresponding eigenvalue ε_j. (For our choice of $V_1(\vec{x})$ and $U(\vec{\xi})$ - Morse and harmonic respectively - the solutions to (31a) and (31b) are known in analytic form. See Appendix B.) Since H_μ and H_m are Hermitian operators, the correspondingly sets of eigenvectors are complete and may also be orthonormalized. Then

$$\left[H_\mu(\vec{\xi}) + H_m(\vec{x})\right]\phi_j(\vec{x})u_v(\vec{\xi}) = (\varepsilon_j + \Delta_v)\phi_j(\vec{x})u_v(\vec{\xi}) \ . \tag{32}$$

We shall now adopt the formalism of second quantization to describe the total system of many gas molecules. The second quantized, many particle, static Hamiltonian is then

$$\hat{H} = \int d\vec{x}\, d\vec{\xi}\, \psi^\dagger(\vec{x},\vec{\xi})H(\vec{x},\vec{\xi})\psi(\vec{x},\vec{\xi}) \ . \tag{33}$$

We expand the field operator in terms of the eigenvectors of $(H_\mu + H_m)$ as

$$\psi(\vec{x},\vec{\xi}) = \sum_{j,v} \phi_j(\vec{x})u_v(\vec{\xi})\, \alpha_j^v \ . \tag{34}$$

$\alpha_j^v(\alpha_j^{v\dagger})$ is the annihilation (creation) operator for a particle in the j^{th} state of the surface potential and in the v^{th} molecular vibrational state. Then, applying (32) through (34) and using the orthonormality of $\{u_n\}$ and $\{\phi_j\}$ leads to

$$(\hat{H}_\mu + \hat{H}_m) \equiv \int d\vec{x}\, d\vec{\xi}\, \psi^\dagger(\vec{x},\vec{\xi})\left[H_\mu(\vec{\xi}) + H_m(\vec{x})\right]\psi(\vec{x},\vec{\xi}) = \sum_{j,v} E_j^v \alpha_j^{v\dagger}\alpha_j^v \tag{35}$$

where $E_j^v = \varepsilon_j + \Delta_v$, and

$$\hat{H}_{res} \equiv \int d\vec{x}\, d\vec{\xi}\, \psi^{\dagger}(\vec{x},\vec{\xi}) H_{res}(\vec{x},\vec{\xi}) \psi(\vec{x},\vec{\xi}) = \sum_{jj'vv'} Z(j,v,j',v) \alpha_j^{v\dagger} \alpha_{j'}^{v'} \quad (36)$$

where

$$Z(j,v,j',v') = \int d\vec{x}\, d\vec{\xi}\, \phi_j^*(\vec{x}) u_v^*(\vec{\xi}) H_{res}(\vec{x},\vec{\xi}) \phi_{j'}(\vec{x}) u_{v'}(\vec{\xi}) \quad (37)$$

§2.3.2 The electromagnetic field interaction

In Section 2.2 the electromagnetic field due to laser radiation in the absence of any gas molecules was determined, with Hamiltonian given by equation (23) as

$$\hat{H}_{em} = \sum_{\beta} \int d\vec{k}\, \Omega_{\vec{k}\beta} \left(C^{\dagger}_{\vec{k}\beta} C_{\vec{k}\beta} + \frac{1}{2} \right) . \quad (38)$$

To calculate the effect of the electromagnetic field on an adsorbed gas molecule, we use the method of minimal coupling[14]. The kinetic momentum $\vec{p}$ of a point particle with charge Q and mass m is replaced by $\vec{p} - Q\vec{A}$, and

$$-\frac{\hbar^2}{2m} \nabla^2 \longrightarrow -\frac{\hbar^2 \nabla^2}{2m} + \frac{i\hbar Q}{m} \vec{A}\cdot\nabla \quad . \quad (39)$$

Assuming that the molecule comprises point particles 1 and 2 with charges Q and -Q, respectively, substitution of (39) into (27) gives

$$H_{st} \longrightarrow H_{st} - i\hbar \frac{Q}{\mu} \vec{A}(\vec{x},t)\cdot\frac{\partial}{\partial\vec{\xi}} \quad . \quad (40)$$

We have made the approximation that, since the radiation wavelength is much larger than $|\vec{\xi}|$, $\vec{A}(\vec{x})$ changes very little over $\vec{\xi}$. Thus

$$\vec{A}(\vec{x}_i) \cong \vec{A}(\vec{x}) \mp \nabla\vec{A}(\vec{x})\cdot\left(\frac{\mu}{m_i}\right)\vec{\xi}$$

where i = 1,2. The laser coupling term is then

$$H_{\ell} = -i\hbar \frac{Q}{\mu} \vec{A}(\vec{x},t)\cdot\frac{\partial}{\partial\vec{\xi}} \quad ,$$

which gives in second quantization

$$\hat{H}_\ell = \int d\vec{x}\, d\vec{\xi}\, \psi^\dagger(\vec{x},\vec{\xi}) H_\ell(\vec{x},\vec{\xi}) \psi(\vec{x},\vec{\xi})$$
$$= -i\hbar \frac{Q}{\mu} \sum_{jj'vv'} \int d\vec{x}\, \phi_j^*(\vec{x}) \vec{A}(\vec{x},t) \phi_{j'}(\vec{x}) \cdot \int d\vec{\xi}\, u_v^*(\vec{\xi}) \frac{\partial}{\partial \vec{\xi}} u_{v'}(\vec{\xi})$$
$$\times \alpha_j^{v\dagger} \alpha_{j'}^{v'} \qquad (41)$$

Now, assuming the adsorbed molecule is localized at a particular site on the surface, we may take $\vec{A}(\vec{x},t) \cong \vec{A}(0,t)$ where the origin is chosen to be on the surface at the adsorption site. Then (41) becomes

$$\hat{H}_\ell = -i\hbar \frac{Q}{\mu} \vec{A}(0,t) \cdot \sum_{jj'vv'} \delta_{jj'} \int d\vec{\xi}\, u_v^*(\vec{\xi}) \frac{\partial}{\partial \vec{\xi}} u_{v'}(\vec{\xi}) \alpha_j^{v\dagger} \alpha_{j'}^{v'} . \qquad (42)$$

(This is the so-called dipole approximation.) Expanding $\vec{A}(\vec{x},t)$ as in (9) and defining

$$\vec{Y}(j,v,j',v') = -i\hbar \sqrt{\frac{\hbar}{2\varepsilon_o}} \frac{Q}{\mu} \delta_{jj'} \int d\vec{\xi}\, u_v^*(\vec{\xi}) \frac{\partial}{\partial \vec{\xi}} u_{v'}(\vec{\xi}) , \qquad (43)$$

one may rewrite the laser interaction term in the Hamiltonian as

$$\hat{H}_\ell = \sum_{jj'vv'} \vec{Y}(j,v,j',v') \alpha_j^{v\dagger} \alpha_{j'}^{v'} \sum_\beta \int d\vec{k}\, \Omega_{\vec{k}\beta}^{-\frac{1}{2}} \left[\vec{U}_{\vec{k}\beta}(0) e^{-i\Omega_{\vec{k}\beta} t} C_{\vec{k}\beta} + h. \right] \qquad (44)$$

§2.3.3 Dynamics of the solid - phonons

An adequate treatment of the solid must not neglect its internal thermal vibrations. We assume that the only relevant effect of these vibrations is to move the surface adjacent to the adsorbate molecule from $\vec{x} = 0$ to $\vec{x} = \vec{a}$. $\vec{a}$ is a function of time and may be expanded in terms of the normal modes, or phonons, of the solid as

$$\vec{a}(t) = \sqrt{\frac{\hbar}{2M_s N_s}} \sum_J \frac{\vec{\varepsilon}_J}{\sqrt{\omega_J}} \left[b_J^\dagger(t) + b_J(t) \right] \qquad (45)$$

where M_s = mass of a solid molecule, N_s = number of molecules in solid,

J is a multi-index identifying the vibrational modes (phonons) of the solid, each of which has annihilation (creation) operator b_J ($b_J^\dagger$), unit polarization vector $\vec{\varepsilon}_J$, and frequency ω_J.

To include the effect of thermal vibrations in the Hamiltonian, let the surface to molecule displacement now be $\vec{x} - \vec{a}(t)$ in equation (28) (and ignore V_2) to get

$$H_{st} \longrightarrow H_{st} + V_1(\vec{x} - \vec{a}(t) - \frac{\mu}{m_1}\vec{\xi}) - V_1(\vec{x} - \frac{\mu}{m_1}\vec{\xi}) \ . \tag{46}$$

Expanding $V_1(\vec{x} - \vec{a}(t) - \frac{\mu}{m_1}\vec{\xi})$ in a Taylor series to first order in $\vec{a}(t)$ gives

$$H_{st} \longrightarrow H_{st} - \vec{a}(t)\cdot\frac{\partial}{\partial\vec{x}} V_1(\vec{x} - \frac{\mu}{m_1}\vec{\xi}) \ . \tag{47}$$

The validity of this approximation, which includes one phonon processes only, is discussed in references 2 and 15. We note here only that the coupling to the phonons in the solid must be weak.

Defining

$$H_{ph} = - \vec{a}(t) \cdot\frac{\partial}{\partial\vec{x}} V_1(\vec{x} - \frac{\mu}{m_1}\vec{\xi}) \tag{48}$$

and using (45), the phonon interaction term in the second quantized Hamiltonian becomes

$$\hat{H}_{ph} = \int d\vec{x}\, d\vec{\xi}\, \psi^\dagger(\vec{x},\vec{\xi})\, H_{ph}\, \psi(\vec{x},\vec{\xi})$$

$$= -\sqrt{\frac{\hbar}{2M_s N_s}} \sum_J \frac{\vec{\varepsilon}_J}{\sqrt{\omega_J}} (b_J^\dagger(t) + b_J(t)) \sum_{jj'vv'} \int\Big[d\vec{x}\, d\vec{\xi}\, \phi_j^*(\vec{x}) u_v^*(\vec{\xi}) \frac{\partial}{\partial\vec{x}}$$

$$\times\ V_1(\vec{x} - \frac{\mu}{m_1}\vec{\xi})\phi_{j'}(\vec{x}) u_{v'}(\vec{\xi})\Big] a_j^{v\dagger} a_{j'}^{v'}$$

or

$$\hat{H}_{ph} = \sum_{jj'vv'} \Big[\vec{X}(j,v,j',v') a_j^{v\dagger} a_{j'}^{v'} \cdot \sum_J \frac{\vec{\varepsilon}_J}{\sqrt{\omega_J}} (b_J^\dagger(t) + b_J(t)\Big] \tag{49}$$

where

$$\vec{X}(j,v,j',v') = -\sqrt{\frac{\hbar}{2M_s N_s}} \int d\vec{x}\, d\vec{\xi}\, \phi_j^*(\vec{x}) u_v^*(\vec{\xi}) \frac{\partial}{\partial \vec{x}} V_1(\vec{x} - \frac{\mu}{m_1}\vec{\xi}) \phi_{j'}(\vec{x}) u_{v'}(\vec{\xi}) . \tag{50}$$

We have assumed here that the phonon spectrum of the solid is essentially unperturbed by the adsorbed molecule, and hence α_j^v commutes with b_J. (This approximation excludes the possibility of heating the solid via this interaction.) The Hamiltonian of the solid is, in the harmonic approximation,

$$\hat{H}_s = \sum_J \hbar\omega_J \left(b_J^\dagger b_J + \frac{1}{2}\right) . \tag{51}$$

§2.3.4 The complete Hamiltonian

We are now prepared to construct the complete Hamiltonian for the dynamical gas-solid-laser system. It is presumed that, initially, (for $t < 0$) equilibrium conditions exist. The initial occupations of states are assumed to be given by $\hat{H}_\mu + \hat{H}_m + \hat{H}_s + \hat{H}_{em}$, which is diagonal in the basis we use. Then at $t = 0$ the laser is turned on, creating a non-equilibrium situation. The subsequent time evolution of the system is determined by the non-diagonal interaction terms $\hat{H}_{ph} + \hat{H}_\ell + \hat{H}_{res}$, so we turn on these terms at $t = 0$.[1] The Hamiltonian may then be written as

$$\hat{H} = \hat{H}_\mu + \hat{H}_m + \hat{H}_s + \hat{H}_{em} + \theta(t)[\hat{H}_{ph} + \hat{H}_\ell + \hat{H}_{res}] . \tag{52}$$

Formally, $\hat{H}_{res}$ should be included as a correction to $\hat{H}_m$ for all times. However, it will be seen in the next section that $\hat{H}_{res}$ does not contribute when the gas molecules are restricted to adsorbed states. This is essentially the case for $t < 0$, since the occupation numbers of the surface states initially follow a Boltzmann distribution and $k_B T << V_o$. (V_o is the depth of the potential well of the surface bond.)

Note also that we have assumed that the laser is kept on throughout the complete desorption process. Thus, when a pulsed laser is used, our theory predicts a desorption rate that carries on for only the duration of the pulse.

§2.4 Calculation of the Transition Rates

§2.4.1 Application of the perturbation theory

In Section 2.1 we proposed to describe the desorption process by the master equation

$$n_j^v(t) = \sum_{(j',v')\neq(j,v)} R_{jj'}^{vv'} n_{j'}^{v'}(t) - \left(\sum_{(j',v')\neq(j,v)} R_{j'j}^{v'v} + \sum_{v'\neq v} R_{cj}^{v'v} \right) n_j^v(t) \quad . \tag{2}$$

We will calculate the contributions to the rates $R_{j'j}^{v'v}$ and $R_{cj}^{v'v}$ due to the interaction terms $\hat{H}_\ell$, $\hat{H}_{ph}$, and $\hat{H}_{res}$ individually. Using Fermi's Golden Rule, (second order time-dependent perturbation theory) the single particle transition rate from state $|a\rangle$ to $|b\rangle$ is given by[16]

$$\omega_{b\leftarrow a} = \frac{2\pi}{\hbar} |\langle b|H_{int}|a\rangle|^2 \, \delta(E_b - E_a) \tag{53}$$

where H_{int} is the interaction term in the Hamiltonian and $E_{(a,b)}$ is the energy level of state (a,b). Equation (53) is valid in the long-time limit, and provided that the interaction (H_{int}) is sufficiently weak.

The state of a single adsorbed gas molecule is described by its surface bond state (j) and internal vibrational state (v) which have, in our approximate model, a separable state function $|j\rangle|v\rangle$. The state of the solid is characterized by its phonon distribution $\{n_J^{ph}\}$, previously assumed to be basically unperturbed by the gas molecules and laser. The laser electromagnetic fields are described by the photon

distribution $\{n^{em}_{\vec{k}\beta}\}$, independently of both phonons and gas molecules. The complete one-gas-molecule+solid+laser system may then be described by the separable state function $|j\rangle|v\rangle|\{n^{ph}_J\}\rangle|\{n^{em}_{\vec{k}\beta}\}\rangle$. We can now apply (53) to our system to calculate the single particle transition rates.

According to (53), the transition rate from (j',v') to (j,v) due to the laser term ($\hat{H}_\ell$) is

$$L^{vv'}_{jj'} = \frac{2\pi}{\hbar} \left| \langle j|\langle v|\langle\{n^{ph}_J\}|\langle\{n^{em}_{\vec{k}\beta}\}|\hat{H}_\ell|j'\rangle|v'\rangle|\{n^{ph}_J\}'\rangle|\{n^{em}_{\vec{k}\beta}\}'\rangle \right|^2$$
$$\times \delta\left(E_{j,v,\{n^{ph}\},\{n^{em}\}} - E_{j',v',\{n^{ph}\}',\{n^{em}\}'}\right) \quad . \qquad (54)$$

Substituting expression (44) for $\hat{H}_\ell$ in (54) and noting that $\hat{H}_\ell$ is independent of phonons, we get, after a few simple algebraic steps,

$$L^{vv'}_{jj'} = \frac{2\pi}{\hbar} \sum_\beta \int d\vec{k} \frac{1}{\Omega_{\vec{k}}} \left| \vec{Y}(j,v,j',v') \cdot \vec{U}_{\vec{k}\beta}(0) \right|^2$$
$$\times \left[n^{em}_{\vec{k}\beta}\, \delta(E^v_j - E^{v'}_{j'} - \hbar\Omega_{\vec{k}}) + (n^{em}_{\vec{k}\beta} + 1)\delta(E^v_j - E^{v'}_{j'} + \hbar\Omega_{\vec{k}}) \right] . \qquad (55)$$

Similarly, we substitute (49) for $\hat{H}_{ph}$ into (53) to get the phonon assisted transition rate,

$$P^{vv'}_{jj'} = \frac{2\pi}{\hbar} \sum_J \frac{1}{\omega_J} \left| \vec{X}(j,v,j',v') \cdot \vec{\varepsilon}_J \right|^2$$
$$\times \left[n^{ph}_J \delta(E^v_j - E^{v'}_{j'} - \hbar\omega_J) + (n^{ph}_J + 1)\ (E^v_j - E^{v'}_{j'} + \hbar\omega_J) \right] . \qquad (56)$$

(We may replace the bound state index j with q to get the transition rate to a continuum state.) Finally, the transition rate due to tunneling via $\hat{H}_{res}$ is calculated by substituting (36) into (53) to get

$$Q^{vv'}_{qj'} = \frac{2\pi}{\hbar} \left| \vec{Z}(q,v,j',v') \right|^2 \delta(E^v_q - E^{v'}_{j'}) \quad . \qquad (57)$$

We assume that the energy levels E^v_j are non-degenerate for all bound states. This is plausible since ε_j and Δ_v take on discrete and un-

related values, so it is highly improbable that $E_j^v - E_{j'}^{v'} = 0$ if both j' and j are bound states. Therefore $Q_{jj'}^{vv'} = 0$. If the final state is in the continuum, it is then possible that $E_q^v - E_{j'}^{v'} = 0$, and hence $Q_{qj'}^{vv'}$ may be non-zero. It should be remarked that Lucas and Ewing[10] have considered desorption due to this tunneling term alone. We will later see how their theory fits into ours.

The calculation of the transition rates $L_{jj'}^{vv'}$, $P_{jj'}^{vv'}$, and $Q_{qj'}^{vv'}$ involves the evaluation of the matrix elements $\vec{Y}(j,v,j',v')$, $\vec{X}(j,v,j',v')$ and $\vec{Z}(j,v,j',v')$, respectively. To simplify the calculations in the following sections, we assume that the axis of the adsorbed diatomic molecule is perpendicular to the surface. We furthermore restrict atoms 1 and 2 to motion along this axis, and take the wave function for the molecule to be one dimensional, hence $\phi_j(\vec{x}) = \phi_j(x)$. This one-dimensional approximation is really more appropriate if the molecule is free to move on the surface, rather than highly localized as we assume here. We do not, however, expect this approximation to affect the results significantly in a qualitative way[17].

§2.4.2 $\vec{Y}(j,v,j',v')$ and $L_{jj'}^{vv'}$

To calculate $L_{jj'}^{vv'}$, we first evaluate $|\vec{Y}(j,v,j',v')\cdot\vec{U}_{k\beta}(0)|^2$ and $n_{\vec{k}\beta}^{em}$, and substitute these expressions into equation (55) for $L_{jj'}^{vv'}$.

$\vec{Y}(j,v,j',v')$, given in (43), is now rewritten in the one dimensional approximation ($\vec{\xi} = \xi\vec{n}$, $\vec{x} = x\vec{n}$) using bra-ket notation as

$$\vec{Y}(j,v,j',v') = -i\hbar\sqrt{\frac{\hbar}{2\varepsilon_o}}\,\frac{Q}{\mu}\,\delta_{jj'}\int d\xi\, u_v^*(\xi)\,\frac{\partial}{\partial\xi}\,u_{v'}(\xi)\vec{n}$$

$$= -i\hbar\sqrt{\frac{\hbar}{2\varepsilon_o}}\,\frac{Q}{\mu}\,\langle v|\frac{\partial}{\partial\xi}|v'\rangle\vec{n}\,\delta_{jj'}\,. \qquad (58)$$

Since the molecular vibrations are assumed to be simple harmonic, we make use of the annihilation (creation) operators a ($a^\dagger$) of harmonic vibrational modes to express

$$\langle v \left| \frac{\partial}{\partial \xi} \right| v' \rangle = \sqrt{\frac{\mu\omega_v}{2\hbar}} \langle v | a - a^\dagger | v' \rangle$$

$$= \sqrt{\frac{\mu\omega_v}{2\hbar}} \left[\sqrt{v+1}\, \delta_{v',v+1} - \sqrt{v}\, \delta_{v',v-1} \right] \qquad (59)$$

where ω_v is the fundamental molecular vibrational frequency. Combining (58) and (59) gives

$$\left| \vec{Y}(j,v,j',v') \cdot \vec{U}_{\vec{k}\beta}(0) \right|^2 = \frac{Q^2 \hbar^2 \omega_v}{4\epsilon_o \mu} \left| \vec{n} \cdot \vec{U}^o_{\vec{k}\beta} \right|^2$$

$$\times \left[(v+1)\delta_{v',v+1} + v\, \delta_{v',v-1} \right] \qquad (60)$$

where $\vec{U}^o_{\vec{k}\beta}$ is $\vec{U}_{\vec{k}\beta}(x)$ evaluated as $x \to 0$ with $x \geq 0$.
(Note that only p-polarized photon modes contribute to (60).)
Substituting (60) into (55) and rewriting the delta functions slightly gives

$$L^{vv'}_{jj'} = \frac{Q^2\pi}{2\epsilon_o \mu c} \int d\vec{k} \left| \vec{n} \cdot \vec{U}^o_{\vec{k}p} \right|^2 \left[n^{em}_{\vec{k}p}\, v\, \delta_{v',v-1} + (n^{em}_{\vec{k}p} + 1)(v+1)\, \delta_{v',v+1} \right]$$

$$\times \delta\left(\frac{\omega_v}{c} - k\right) \delta_{jj'} \, . \qquad (61)$$

It is convenient to introduce polar coordinates in (61) as $\vec{k} \to k\hat{k}$ to get

$$L^{vv'}_{jj'} = \frac{Q^2\pi}{2\epsilon_o \mu c}\, \delta_{jj'} \int_0^\infty dk\, k^2\, \delta\left(\frac{\omega_v}{c} - k\right) \int_{\zeta<0} d\hat{k} \left| \vec{n} \cdot \vec{U}^o_{\hat{k}p} \right|^2$$

$$\times \left[n^{em}_{\hat{k}p}\, v\, \delta_{v',v-1} + (n^{em}_{\hat{k}p} + 1)(v+1)\, \delta_{v',v+1} \right] . \qquad (62)$$

Suppose the laser radiation is strongly concentrated about one direction, $\hat{k}_o$, so $n^{em}_{\hat{k}p}$ is sharply peaked. The slowly varying term $\left| \vec{n} \cdot \vec{U}^o_{\hat{k}p} \right|^2$ may then, to a good approximation, be removed from under the

integral over solid angle $\hat{k}$. The integral over k is easily evaluated using the delta function, leading to

$$L_{jj'}^{vv'} = \frac{Q^2 \pi \omega_v^2}{2\varepsilon_o \mu c^3} \delta_{jj'} \left\{ \left| \vec{n} \cdot \vec{U}^o_{\frac{\omega_v}{c}, \hat{k}_o, p} \right|^2 \left[v\delta_{v',v-1} + (v+1)\delta_{v',v+1} \right] \int_{\zeta<0} d\hat{k}\, n^{em}_{\frac{\omega_v}{c}, \hat{k}, p} \right.$$

$$\left. + (v+1)\delta_{v',v+1} \int_{\zeta<0} d\hat{k} \left| \vec{n} \cdot \vec{U}^o_{\frac{\omega_v}{c}, \hat{k}, p} \right|^2 \right\} \qquad (63)$$

It is useful to express $n^{em}_{\vec{k}\beta}$ in terms of an easily measured quantity, such as the incident laser intensity (I) which we take to be the amplitude of the incident Poynting vector. For plane waves in a vacuum one has

$$I = |\vec{S}|_{ave} = \sqrt{\frac{\varepsilon_o}{\mu_o}} \, |\vec{E}^i(\vec{x},t)|^2_{ave} \qquad (64)$$

where "ave" means the time average and superscript "i" means that only the incident component of the wave is included. Considering now the contribution due to the incident portion of a single mode $(\vec{k}\beta)$, equations (7) and (9) in (64) yield

$$I_{\vec{k}\beta} = c |\vec{U}^i_{\vec{k}\beta}|^2 [\hbar\Omega_{\vec{k}\beta} (n^{em}_{\vec{k}\beta} + \tfrac{1}{2})] \quad . \qquad (65)$$

Note that this is just the energy density times the wave velocity. Ignoring the zero point energy contribution, (65) may be rewritten as

$$n^{em}_{\vec{k}\beta} = \frac{I_{\vec{k}\beta}}{c\hbar\Omega_{\vec{k}\beta} |\vec{U}^i_{\vec{k}\beta}|^2} \quad . \qquad (66)$$

(This approximation is valid since we find $n^{em}_{\vec{k}\beta} >> 1$.)
Since $I_{\vec{k}\beta}$ is sharply peaked about $\hat{k}_o$ and $|\vec{U}^i_{\vec{k}\beta}|$ is much more slowly varying, we get approximately

$$\int_{\zeta<0} d\hat{k}\; n^{em}_{\frac{\omega_v}{c},\hat{k},p} = \frac{1}{\hbar c\omega_v}\;\frac{1}{\left|\vec{U}^{i}_{\frac{\omega_v}{c},\hat{k}p}\right|^2}\int_{\zeta<0} d\hat{k}\; I_{\frac{\omega_v}{c},\hat{k}} = \frac{c^2 I_o g(\omega_v)}{2\hbar\omega_v^3\left|\vec{U}^{i}_{\frac{\omega_v}{c},\hat{k}p}\right|^2} \qquad (67)$$

To arrive at the second equality above, we have taken the total laser intensity to be I_o with normalized frequency distribution $g(\Omega)$. The factor of 1/2 is due to the fact that only p-modes contribute to the interaction, but we assume that the laser radiation is unpolarized. Substituting (67) into (63) we get

$$L^{vv'}_{jj'} = \frac{Q^2\pi\omega_v^2}{2\varepsilon_o\mu c^3}\,\delta_{jj'}\left\{\frac{c^2}{2\hbar\omega_v^3}\left|\frac{\vec{n}.\vec{U}^{o}_{\frac{\omega_v}{c},\hat{k}_o,p}}{\vec{U}^{i}_{\frac{\omega_v}{c},\hat{k}_o,p}}\right|^2 I_o g(\omega_v)\right.$$

$$\left.\times\left[v\delta_{v',v-1} + (v+1)\delta_{v',v+1}\right] + (v+1)\delta_{v',v+1}\int_{\zeta<0} d\hat{k}\left|\vec{n}.\vec{U}^{o}_{\frac{\omega_v}{c},\hat{k},p}\right|^2\right\} \qquad (68)$$

(photon absorption) (stimulated emission) (spontaneous emission)

To proceed further, details of the laser radiation must be specified. At normal laser intensities, the last term in (68) - due to spontaneous photon emission- can be safely ignored. We shall also take the frequency distribution to be Lorentzian, centred on the molecular vibrational frequency, ω_v. That is,

$$g(\Omega) = \frac{1}{\pi}\;\frac{\gamma/2}{(\Omega-\omega_v)^2 + (\gamma/2)^2} \qquad (69)$$

where γ is the half-width of the frequency distribution. If the laser is in continuous wave operation, then γ is the line width of the radiation associated with decay processes of time constant τ_ℓ. On the other hand, a laser in pulsed operation - "Q-switched" with pulse duration $\tau_p \sim 100$ ns - will have frequency spread given by the Fourier transform

of the pulse shape, and hence $\gamma \sim \tau_p^{-1}$. (We assume that the frequency spread due to the pulse shape dominates over all other sources of line broadening; that is, $\tau_p \ll \tau_\ell$.) In either case, the frequency distribution may not be Lorentzian, but the error introduced here is small. Equation (68) then becomes

$$L_{jj'}^{vv'} = \frac{Q^2}{2\varepsilon_o \mu c \hbar \omega_v} (I_o \tau) \left| \frac{\vec{n} \cdot \vec{U}^o_{\frac{\omega_v}{c}, \hat{k}_o, p}}{\vec{U}^i_{\frac{\omega_v}{c}, \hat{k}_o, p}} \right|^2 \left[v\delta_{v',v-1} + (v+1)\delta_{v',v+1} \right] \delta_{jj'} \tag{70}$$

For a pulsed laser, we let the pulse fluence be $F_\ell = I_o \tau$. (In fact, in the case of continuous wave laser operation, we may use the term "fluence" as defined above to mean the intensity times inverse line width.)

For our dielectric solid, equations (13a,b) give

$$\left| \frac{\vec{n} \cdot \vec{U}^o_{\frac{\omega_v}{c}, \hat{k}_o, p}}{\vec{U}^i_{\frac{\omega_v}{c}, \hat{k}_o, p}} \right|^2 = \frac{4n_r^2 \sin^2\theta}{\left[n_r + \sqrt{1 + (1 - 1/n_r^2)\tan^2\theta} \right]^2} \,. \tag{71}$$

(Note that, as $n_r \to 1$, (71) $\to \sin^2\theta$. This is just what one expects in an infinite vacuum without the solid.) The final expression for the transition rate is

$$L_{jj'}^{vv'} = \frac{Q^2}{2\varepsilon_o \mu c \hbar \omega_v} \frac{4n_r^2 \sin^2\theta}{\left[n_r + \sqrt{1 + (1 - 1/n_r^2)\tan^2\theta} \right]^2} \times F_\ell \left[v\delta_{v',v-1} + (v+1)\delta_{v',v+1} \right] \delta_{jj'} \,. \tag{72}$$

From the form of $L_{jj'}^{vv'}$ above, it is clear that the photon interaction induces one-step transitions between vibrational (v) states, but does not affect the surface state (j).

As an aside, we note that, if the solid were instead a perfect conductor, one must use equation (24) to replace the form factor (71) in (72) with

$$\left| \frac{\vec{n}.\vec{U}^{o}_{\omega_{\frac{v}{c}},\hat{k}_o,p}}{\vec{U}^{i}_{\omega_{\frac{v}{c}},\hat{k}_o,p}} \right|^2 = 4 \sin^2 \theta \quad . \tag{73}$$

Both form factors give zero contribution at perpendicular incidence ($\theta = 0$). While the form factor for the perfect conductor is largest at grazing incidence, the dielectric form factor is maximized at an intermediate angle. See Fig. 6 in which (71) and (73) are compared graphically.

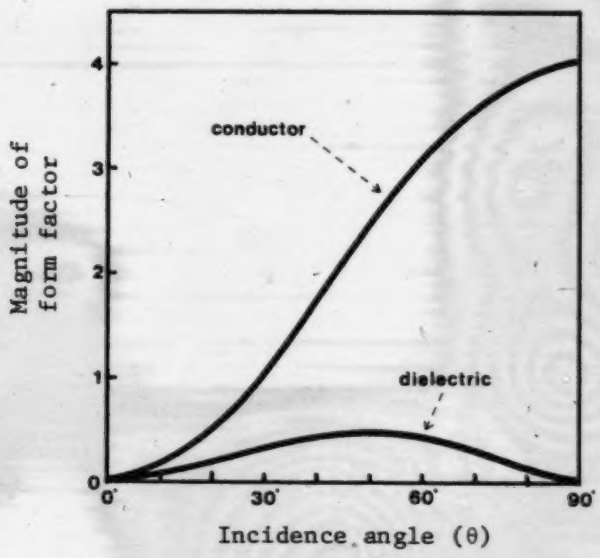

Fig. 6. Angular dependence of the vibrational transition rate.

§2.4.3 The phonon interaction; $\vec{X}$ and $P^{vv'}_{jj'}$

i) Bound state-bound state transitions

We shall now calculate the transition rates due to the phonon interaction, $\hat{H}_{ph}$. First, consider transitions among bound surface states only.

The phonon-assisted transition rate, $P^{vv'}_{jj'}$, given in (56), depends on the matrix element $\vec{X}(j,v,j',v')$. In our one-dimensional theory (50) becomes

$$\vec{X}(j,v,j',v') = -\left(\frac{\hbar}{2M_s N_s}\right)^{\frac{1}{2}} \int dx\, \phi_j^*(x) \langle v| \frac{\partial}{\partial x} V_1(x - \frac{\mu}{m_1}\xi) |v'\rangle \phi_{j'}(x) \vec{n}. \quad (74)$$

We choose to use a Morse surface potential extending perpendicularly to the surface. Hence

$$V_1(x) = V_o(e^{-2\gamma(x-x_o)} - 2e^{-\gamma(x-x_o)}). \quad (75)$$

This potential has a maximum depth of V_o at x_o and a range given by γ^{-1}. Provided we have $x_o \geq \gamma^{-1}$, so V_1 increases rapidly for $x \leq 0$, we expect this potential to be realistic[1]. In Appendix B the energy eigenvalues and wave functions of this potential are listed.

Expanding $V_1(x - \frac{\mu}{m_1}\xi)$ in a Taylor series about $x - \frac{\mu}{m_1}\xi_o$ in (74) gives

$$\vec{X}(j,v,j',v') = 2V_o\gamma\left(\frac{\hbar}{2M_s N_s}\right)^{\frac{1}{2}} \sum_{\ell=0}^{\infty} \frac{1}{\ell!} \left(\frac{\mu\gamma}{m_1}\right)^{\ell} I_{\ell jj'} \langle v| (\xi-\xi_o)^{\ell} |v'\rangle \vec{n} \quad (76a)$$

where

$$I_{\ell jj'} = \int_{\zeta_o=-\gamma(x_o+\frac{\mu}{m_1}\xi_o)}^{\infty} d\zeta\, \phi_j^*(\zeta) e^{-\zeta}(2^{\ell}e^{-\zeta} - 1)\phi_{j'}(\zeta) \quad (76b)$$

and $\phi_j(\zeta-\zeta_o) = \gamma^{-\frac{1}{2}}\phi_j(x)$. These bound state Morse wave functions are given in Appendix B, and $I_{\ell jj'}$ is evaluated in Appendix C. The

dimensionless integration variable in (76b) is $\zeta = \gamma(x - x_o - \frac{\mu}{m_1}\xi_o)$. We choose the lower limit of integration - equivalent to $x = 0$ - to imply that the gas particles do not penetrate the solid. Since the v states are those of a harmonic oscillator, we express the coordinate $\xi - \xi_o$ as $\xi - \xi_o = \sqrt{\frac{\hbar}{2\mu\omega_v}}(a + a^\dagger)$ and expand $\langle v|(a+a^\dagger)^\ell|v'\rangle = \langle v|(a^\dagger)^\ell|v'\rangle + \langle v|a(a^\dagger)^{(\ell-1)}|v'\rangle + \ldots$, to find that, for $v > v'$,

$$\vec{X}(j,v,j',v') = 2\gamma V_o \left(\frac{\hbar}{2M_s N_s}\right)^{\frac{1}{2}} \left(\frac{v!}{v'!}\right)^{\frac{1}{2}} \frac{1}{(v-v')!} \left(\frac{\mu\gamma^2\hbar}{2m_1^2\omega_v}\right)^{\frac{v-v'}{2}} \vec{n}$$

$$\times \left[I_{(v-v')jj'} + \left(\frac{\mu\gamma^2\hbar}{2m_1^2\omega_v}\right) \frac{v+1}{(v-v'+1)(v-v'+2)} I_{(v-v'+2)jj'} + \ldots \right] \quad (77)$$

But $\left(\frac{\mu\gamma^2\hbar}{2m_1^2\omega_v}\right) \ll 1$, so we may write, to a good approximation,

$$\vec{X}(j,v,j',v') = 2\gamma V_o \left(\frac{\hbar}{2M_s N_s}\right)^{\frac{1}{2}} \left(\frac{v_>!}{v_<!}\right)^{\frac{1}{2}} \frac{1}{|v-v'|!} \left(\frac{\mu\gamma^2\hbar}{2m_1^2\omega_v}\right)^{\frac{|v-v'|}{2}} I_{|v-v'|jj'} \vec{n} \quad (78)$$

where $v_>(v_<)$ is the greater (lesser) of (v,v').

To perform the sum in (56), we must know the phonon distribution at the solid surface. This has been calculated by Ezawa[18], and used in previous desorption calculations by Goldys, Gortel and Kreuzer[17]. However, they found that the numerical results differ only slightly from the parallel calculation done using the bulk Debye phonons appropriate for an infinite solid. We will simply use bulk phonons here and expect our results to be qualitatively correct. The phonon index (J) then describes the phonon momentum $(\vec{p})$ and polarization (σ). For the Debye model, we may substitute

$$\sum_J \longrightarrow \frac{3N_s}{\omega_D^3} \int_0^{\omega_D} \omega^2 \, d\omega \ ,$$

which absorbs the $\vec{n}.\vec{\varepsilon}_J$ factor in (56).[19] Using (78), and splitting the transition rate into parts involving phonon emission and absorption, we get

$$P^{vv'}_{jj'} = {}_{em}P^{vv'}_{jj'} + {}_{abs}P^{vv'}_{jj'} \tag{79}$$

where

$${}_{em}P^{vv'}_{jj'} = \frac{6\pi N_s}{\hbar^3\omega_D^3}\left[n^{ph}(E^{v'}_{j'}-E^{v}_{j})+1\right]\left|X(j,v,j',v')\right|^2(E^{v'}_{j'}-E^{v}_{j}) \times \theta(\hbar\omega_D - E^{v'}_{j'}+E^{v}_{j})\,\theta(E^{v'}_{j'}-E^{v}_{j}) \tag{80}$$

$${}_{abs}P^{vv'}_{jj'} = \frac{6\pi N_s}{\hbar^3\omega_D^3}\, n^{ph}(E^{v}_{j}-E^{v'}_{j'})\left|X(j,v,j',v')\right|^2 (E^{v}_{j}-E^{v'}_{j'}) \times\theta(\hbar\omega_D - E^{v}_{j}+E^{v'}_{j'})\,\theta(E^{v}_{j}-E^{v'}_{j'}) \ . \tag{81}$$

The θ-functions ensure that the initial and final molecular states (j,v) differ by at most one Debye energy. The phonons obey Bose statistics, so n^{ph} is the Boson occupation number in thermal equilibrium.

It is useful to scale all rates by the Debye frequency, ω_D, and introduce the dimensionless quantities,

$$\sigma_o = \sqrt{\frac{2mV_o}{\hbar^2\gamma^2}} \qquad \text{and} \qquad r = \frac{2m\omega_D}{\hbar\gamma^2} \ . \tag{82}$$

(σ_o is approximately equal to the number of bound states in the surface potential. See Appendix B.) The energies are all scaled by the Debye energy, $\hbar\omega_D$.

Using the results of Appendix C, (80) and (81) may be rewritten as

$${}_{em}P^{vv'}_{jj'} = F^{vv'}_{jj'}\left[n^{ph}(\varepsilon^{v'}_{j'}-\varepsilon^{v}_{j})+1\right]\theta(1-\varepsilon^{v'}_{j'}+\varepsilon^{v}_{j})\,\theta(\varepsilon^{v'}_{j'}-\varepsilon^{v}_{j}) \tag{83a}$$

$${}_{abs}P^{vv'}_{jj'} = F^{vv'}_{jj'}\, n^{ph}(\varepsilon^{v}_{j}-\varepsilon^{v'}_{j'})\,\theta(1-\varepsilon^{v}_{j}+\varepsilon^{v'}_{j'})\,\theta(\varepsilon^{v}_{j}-\varepsilon^{v'}_{j'}) \tag{83b}$$

where

$$F^{vv'}_{jj'} = \omega_D \frac{24\pi\sigma_o^2}{r^3} \frac{m}{M_s} \frac{v_>!}{v_<!} \frac{1}{(|v-v'|!)^2} \left(\frac{4m_2/m_1}{r\delta_v}\right)^{|v-v'|} \frac{j_>!\Gamma(2\sigma_o - j_>)}{j_<!\Gamma(2\sigma_o - j_<)}$$

$$\times (\sigma_o - j - \tfrac{1}{2})(\sigma_o - j' - \tfrac{1}{2})(j - j')^2 \left[(v'-v)\delta_v + \frac{1}{r}(j'-j)(2\sigma_o - j - j' - 1)\right]$$

$$\times \left(\frac{2\sigma_o - j - j' - 1}{2\sigma_o} + \frac{1 - 2^{-|v-v'|}}{|j - j'|}\right)^2 \qquad (84)$$

and $\delta_v = \frac{\omega_v}{\omega_D}$ = fundamental molecular vibrational frequency in units of ω_D;

$j_>(j_<)$ is the greater (lesser) of (j, j');

$$\varepsilon^{v'}_{j'} - \varepsilon^{v}_{j} = (v' - v)\delta_v + \frac{1}{r}(j'-j)(2\sigma_o - j - j' - 1);$$

$$n^{ph}(\varepsilon) = \frac{1}{e^{\delta\varepsilon} - 1} \quad ; \qquad \delta = \frac{\hbar\omega_D}{k_B T} \quad .$$

Notice that the transition rates decrease rapidly as $|v-v'|$ increases because of the small factor $((4m_2/m_1)/r\delta_v) << 1$. The collection of gamma functions from $\vec{X}(j,v,j',v')$ involving j and j' has been shown[20] to strongly favour transitions where j and j' differ by one. This encourages a cascade of step by step transitions through the bound states.

ii) Bound state to continuum transitions

The total phonon-assisted transition rate from a particular bound state (j',v') to any continuum state with vibrational index v is

$$P^{vv'}_{cj'} = \sum_q P^{vv'}_{qj'} \qquad (85)$$

where the surface state label q is the (one-dimensional) wave vector of the free (desorbed) particle. Using (56) we have

$$P^{vv'}_{cj'} = \frac{2\pi}{\hbar} \sum_q \sum_J \frac{1}{\omega_J} \left| \vec{X}(q,v,j',v') \cdot \vec{\varepsilon}_J \right|^2$$

$$\times \left[n^{ph}_J \delta(E^v_q - E^{v'}_{j'} - \hbar\omega_J) + (n^{ph}_J + 1)\delta(E^v_q - E^{v'}_{j'} + \hbar\omega_J) \right] . \qquad (86)$$

Proceeding similarly to above in (i), we use bulk Debye phonons and pass to the continuum in q to get, after some computation,

$$P^{vv'}_{cj'} = {}_{em}P^{vv'}_{cj'} + {}_{abs}P^{vv'}_{cj'} \qquad (87)$$

where

$${}_{em}P^{vv'}_{cj'} = C^{vv'}_{j'} \int_{\varepsilon^{v'}_{j'} - v\delta_v - 1}^{\varepsilon^{v'}_{j'} - v\delta_v} dx\, \theta(x)\, W^{vv'}_{j'}(x) (\varepsilon^{v'}_{j'} - v\delta_v - x)$$

$$\times [n^{ph}(\varepsilon^{v'}_{j'} - v\delta_v - x) + 1] \qquad (88a)$$

$${}_{abs}P^{vv'}_{cj'} = C^{vv'}_{j'} \int_{\varepsilon^{v'}_{j'} - v\delta_v}^{\varepsilon^{v'}_{j'} - v\delta_v + 1} dx\, \theta(x)\, W^{vv'}_{j}(x) (x - \varepsilon^{v'}_{j'} + v\delta_v) n^{ph}(x - \varepsilon^{v'}_{j'} + v\delta_v) \qquad (88b)$$

with

$$C^{vv'}_{j'} = \omega_D \frac{3\pi}{4} \frac{m}{M_s} \frac{v_>!}{v_<!} \frac{1}{(|v-v'|!)^2} \left| \frac{4m_2/m_1}{r\delta_v} \right|^{|v-v'|} \frac{2\sigma_o - 2j' - 1}{j'!\Gamma(2\sigma_o - j')} \qquad (89a)$$

$$W^{vv'}_{j'} = \left| \Gamma(\sigma_o + \tfrac{1}{2} + i\sqrt{rx}) \right|^2 \frac{\sinh(2\pi\sqrt{rx})}{\cos^2(\pi\sigma_o) + \sinh^2(\pi\sqrt{rx})}$$

$$\times \left\{ x + \frac{1}{r} \left[(\sigma_o - j' - \tfrac{1}{2})^2 + 2\sigma_o (1 - 2^{-|v-v'|}) \right] \right\}^2 \qquad (89b)$$

and

$$\varepsilon^{v'}_{j'} - v\delta_v = -\frac{1}{r} (\sigma_o - j' - \tfrac{1}{2})^2 + (v' - v)\delta_v .$$

The integration variable (x) in (88) and (89) is the kinetic energy of the desorbing particle, scaled by the Debye energy ($\hbar\omega_D$). The limits of integration combined with the theta function allow desorption to a state (q,v) via phonon absorption if the available

energy ($\varepsilon_{j'}^{v'} - v\delta_v$) is with 1 (Debye energy) of the continuum ($\varepsilon = 0$). (That is, $\varepsilon_{j'}^{v'} - v\delta_v + 1 > 0$.) Desorption with phonon emission can occur if $\varepsilon_{j'}^{v'} - v\delta_v > 0$. The form of the factors in (87) to (89) is similar to that in (83) and (84) for bound state to bound state transitions. The matrix element $\vec{X}(q,v,j',v')$ encourages transitions in which the v index varies as little as possible and in which j is as close to the continuum as possible.

§2.4.4 The tunneling transition; $Q_{cj'}^{vv'}$

As explained in Section 2.4.1, the tunneling process due to $\hat{H}_{res}$ can cause bound state to continuum transitions only. In analogy to the phonon assisted rates of the last section, we let the tunneling rate to the continuum be

$$Q_{cj'}^{vv'} = \sum_q Q_{qj'}^{vv'} = \frac{2\pi}{\hbar} \sum_q |Z(q,v,j',v')|^2 \delta(E_q^v - E_{j'}^{v'}) \ . \qquad (90)$$

(To arrive at the second equality, we have substituted equation (57) for $Q_{qj'}^{vv'}$.)

In one dimension, and using a Taylor expansion of $\hat{H}_{res}$ (29) in $Z(q,v,j',v')$ (37) leads to

$$Z(q,v,j',v') = \frac{2V_o}{\sqrt{\gamma}} \sum_{\ell=1}^{\infty} \frac{1}{\ell!} \left(\frac{\mu\gamma}{m_1}\right)^{\ell} I_{(\ell-1)qj'} \langle v|(\xi-\xi_o)^{\ell}|v'\rangle \ . \qquad (91)$$

This equation is similar in form to (76a) for $\vec{X}(j,v,j',v')$. The integral $I_{\ell qj'}$ is the same as $I_{\ell jj'}$ in (76b), except that the bound state wave function for j is replaced by the continuum state function for q. This integral is very similar to one calculated for reference 1, so only the result is quoted in Appendix C.

Performing on (91) the same manipulations that took (76a) into (78) in Section 2.4.3 and substituting into (90) after evaluating the delta function gives

$$Q_{cj'}^{vv'} = \omega_D r \frac{\pi}{16} \frac{v_>!}{v_<!} \frac{1}{(|v-v'|!)^2} \left(\frac{4m_2/m_1}{r\delta_v}\right)^{|v-v'|} \frac{2\sigma_o - 2j' - 1}{j'!\Gamma(2\sigma_o - j')}$$

$$\times \left|\Gamma\left(\sigma_o + \tfrac{1}{2} + i\sqrt{r(\varepsilon_{j'}^{v'} - v\delta_v)}\right)\right|^2 \frac{\sinh\left(2\pi\sqrt{r(\varepsilon_{j'}^{v'} - v\delta_v)}\right)}{\cos^2(\pi\sigma_o) + \sinh^2\left(\pi\sqrt{r(\varepsilon_{j'}^{v'} - v\delta_v)}\right)}$$

$$\times \left[(v'-v)\delta_v + \frac{2\sigma_o}{r}\left(1 - 2^{1-|v-v'|}\right)\right]^2 \theta(\varepsilon_{j'}^{v'} - v\delta_v) \ . \qquad (92)$$

Although we express the rate in (92) in terms of the parameters ω_D and r for convenience, it must be remembered that no phonon processes are involved here. Rather, this process involves a direct tunneling of energy between vibrational (v) states and surface states (j). The remarkable similarity of the components of $Q_{cj'}^{vv'}$, (92) and $P_{cj'}^{vv'}$, (87-89) is due to the very similar forms of the matrix elements Z and $\vec{X}$. ($\vec{X}$ involves the ℓ^{th} derivative of the surface potential while Z contains the $(\ell-1)^{st}$.)

This completes our use of the microscopic, quantum-mechanical theory. We can now construct the full transition rates that appear as coefficients in the matrix of rate equations in (2) or (4). The bound state to bound state transition rate is

$$R_{jj'}^{vv'} = L_{jj'}^{vv'} + P_{jj'}^{vv'} \qquad (93)$$

while the bound state to continuum rate is

$$R_{cj'}^{vv'} = Q_{cj'}^{vv'} + P_{cj'}^{vv'} \ . \qquad (94)$$

§2.5 Solution of the Master Equation

To study the time evolution of the adsorbate, we will solve the rate equations

$$\dot{\vec{n}}(t) = \overleftrightarrow{R}\,\vec{n}(t) \ , \tag{4}$$

subject to the initial conditions

$$n_j^v(0) = N(0)\, e^{-(E_j^v - \mu_g)/k_B T} \ .$$

$N(0)$ is the initial population of the adsorbate and μ_g is the chemical potential of the gas[1]. (The initial distribution of occupation numbers in thermal equilibrium is given, for low particle densities, by the Boltzmann distribution above.)

We follow the method of reference 1 and solve (4) by diagonalization of the matrix $\overleftrightarrow{R}$. Suppose $\overleftrightarrow{R}$ has eigenvalues λ_i and eigenvectors $\vec{e}^{\,i}$. It is then shown in reference 1, by basic linear algebra, that the adsorbate population is given by

$$\frac{N(t)}{N(0)} = \sum_{j,v} \frac{n_j^v(0)}{N(0)} = \sum_i s_i\, e^{\lambda_i t} \qquad \text{(we find } \lambda_i < 0.\text{)} \tag{95}$$

where

$$s_i = \sum_{j,v} \frac{n_j^v(0)}{N(0)}\, \tilde{e}^{\,i}_{jv} \sum_{j'v'} e^{i}_{j'v'}$$

with e^{i}_{jv} = the (j,v) component of $\vec{e}^{\,i}$, and $\sum_{j,v} \tilde{e}^{\,i}_{jv} e^{j'}_{jv} = \delta_{ij'}$.
Now, let the eigenvalue of smallest magnitude be λ_o. Then, as $t \to \infty$,

$$\frac{N(t)}{N(0)} \sim s_o\, e^{\lambda_o t} \tag{96}$$

where $\lambda_o < 0$. That is, at large times, the desorption rate may be characterized by the smallest eigenvalue, λ_o, if s_o is not too small. In

practice, we find by numerical calculation that s_o is usually very close to unity and all other s_i's are normally much smaller in magnitude. In this case the relaxation-time form given in (96) describes the desorption process well. Often we find a few other s_i's are significant too, in which case the desorption process involves several different time scales.

The determination of the s_i and λ_i values is a lengthy numerical calculation, involving the diagonalization of the rather large matrix $\overleftrightarrow{R}$, and the inversion of the matrix of eigenvectors. To keep the matrix size finite, the spectrum of vibrational levels is cut off at an upper limit (v_{max}). Vibrational states are then restricted to $v = 0,1,2,\ldots,$ v_{max}. Such a cut-off is not in principle unreasonable. The interatomic potential of a real molecule is in fact anharmonic, so the higher excited states are not evenly spaced. A laser tuned into the evenly spaced low energy levels will therefore be unable to resonantly excite the higher levels. The exact level at which this cut-off occurs will depend on the laser line width and on the degree of anharmonicity.

In the next section, we will perform the numerical calculation outlined above on several systems of specific interest.

§3. NUMERICAL RESULTS AND DISCUSSION

§3.1 Characterization of our Photodesorption Model

The behaviour of our photodesorption model must now be examined, before theoretical predictions may be compared with experimental results as detailed in the next section. Our theory is first applied to a set of model gas-solid systems for detailed study. The system parameters are

i) the fundamental vibrational frequency (ω_v) of the adsorbate molecule, its atomic masses (m_1,m_2) and dipole charge separation (Q),

ii) the depth (V_o) and range (γ^{-1}) of the surface potential,

iii) the dielectric constant (n_r), molecular mass (M_s) and Debye temperature (T_D) of the solid, and

iv) the laser "fluence" ($F_\ell \equiv$ intensity × inverse line width), and incidence angle (θ).

(Note that we will replace V_o and T_D with the scaled parameters, σ_o and r as defined in equation (82).)

The system parameters are chosen to model the physisorption of CH_3F on an NaCl surface, insofar as the experimental values are known. The CH_3F molecule is believed to adsorb with the F atom closest to the surface and the CH_3 complex sticking outwards. (The laser excites the C-F bond.) The adsorbate molecule and solid parameters (i and iii above) are, with the exception of Q, generally all known. The value of Q is estimated from free space measurements of the C-F bond dipole moment in the gaseous CH_3F molecule[21]. While it is known how the C-F bond vibrational frequency changes as the molecule is brought up against

the surface, the effect on Q is unmeasured. The error in Q introduced here, however large, will affect our results by simply rescaling the fluence axis of the graphs.

There is also some difficulty in describing the surface potential. The well depth (V_o) may be readily estimated from the heat of adsorption as determined by thermal kinetics experiments[3]. The range (γ^{-1}) of the potential is not so easily determined from experimental data. We therefore choose three different values for γ and investigate the desorption kinetics in each case.

In Table 1, parameters for the three systems are listed. We let V_o = 22.5 kJ/mole and γ^{-1} = .35, .25, and .15 Å in systems A, B and C respectively. While the lower two γ^{-1} values are somewhat smaller than

Table 1. System parameters for CH_3F on NaCl.

System	γ^{-1} (Å)	σ_o	r
A	.35	22.8	53.9
B	.25	16.3	27.5
C	.15	8.15	6.9

Other parameters are:

T_D = 281 K , n_r = 1.55 , δ_v = 4.98,
θ = 60° , Q = 1 el. charge.

what one might expect to find physically, these three systems show the varied results attainable using our model. The energy spectra of the corresponding surface potentials are shown in Fig. 7.

By way of introduction, we first consider system A, which is characterized by the parameters $\sigma_o = 22.8$, $r = 53.9$, and $\gamma^{-1} = .35$ Å. The energy spacing between adjacent surface states is always less than one Debye energy, so purely thermal desorption via one-phonon processes is possible.

Using the method described in Section 2, the desorption rate is calculated as a function of fluence and temperature*. Then log rate is graphed against log fluence for various temperatures in Fig. 8; the data is redisplayed in log rate versus inverse temperature graphs in Fig. 9. On the latter graph we include an estimate for purely thermal desorption, without the laser or the vibrational coupling. This is accomplished by including only the phonon-assisted rates $P^{oo}_{jj'}$ and $P^{oo}_{cj'}$ in the calculation, which is precisely the thermal desorption calculation of reference 1. The thermal desorption graph is a straight line, indicating an Arrhenius form for the rate (see Introduction), with the heat of desorption approximately equal to the depth of the lowest bound state.

The photodesorption graphs show enhanced desorption rates at low temperatures. At 100 K, photodesorption occurs at a rate 100 times

*We set $v_{max} = 2$ for the calculations in this section. A molecule in the surface ground state ($j = 0$) needs a minimum vibrational excitation of $v = 2$ to bring its total energy into a degeneracy with the continuum states. We find that the photodesorption rates are greatly hindered if v_{max} is reduced below this level. Increasing v_{max} above 2 results in a slight enhancement of the rates, with no qualitative difference. We prefer to keep $v_{max} = 2$ here in order to reduce the complexity of the numerics to a minimum.

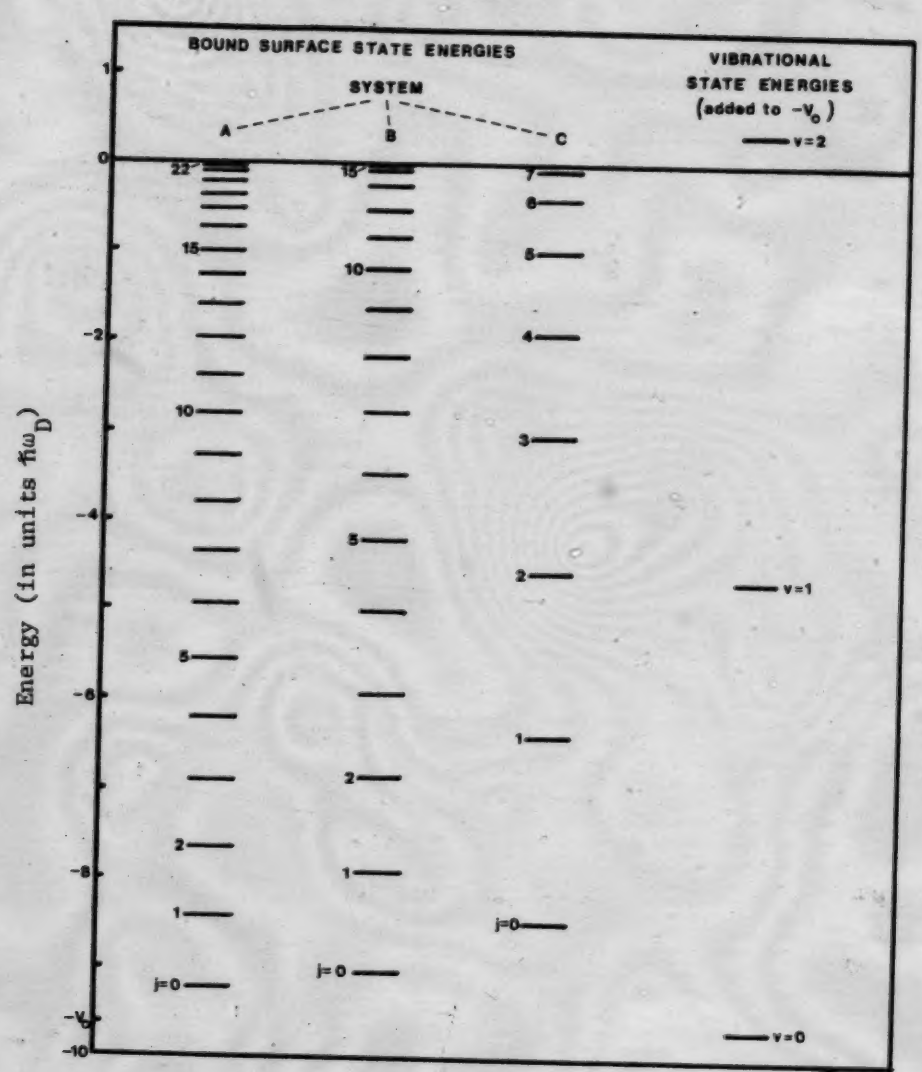

Fig. 7. Energy levels for the CH_3F/NaCl systems A, B, and C.

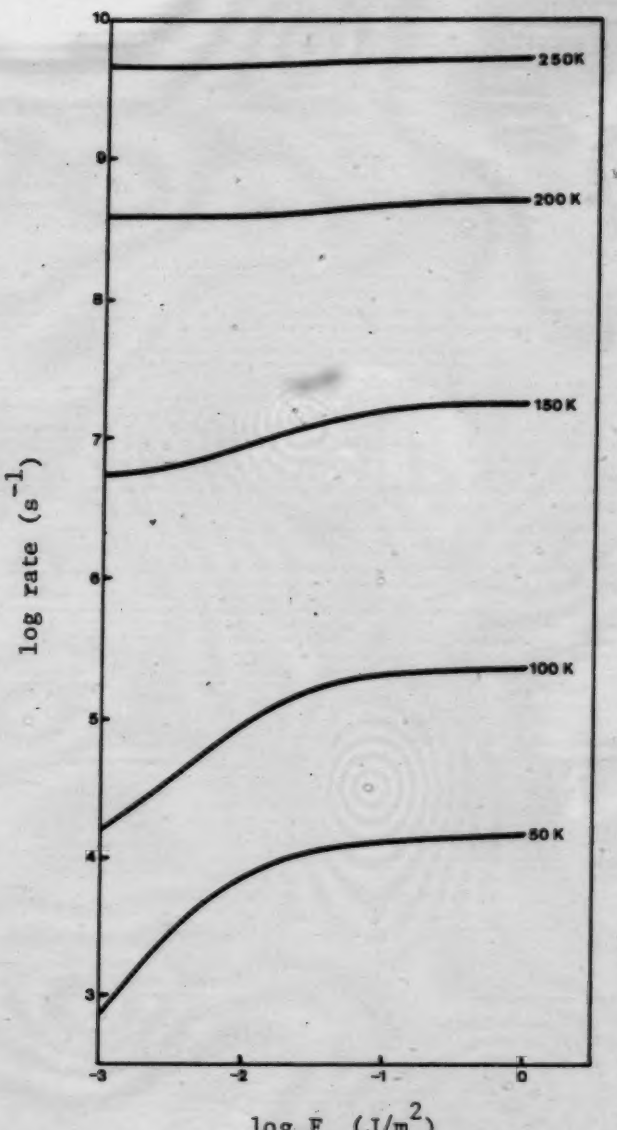

Fig. 8. Log rate versus log fluence for system A at various temperatures.

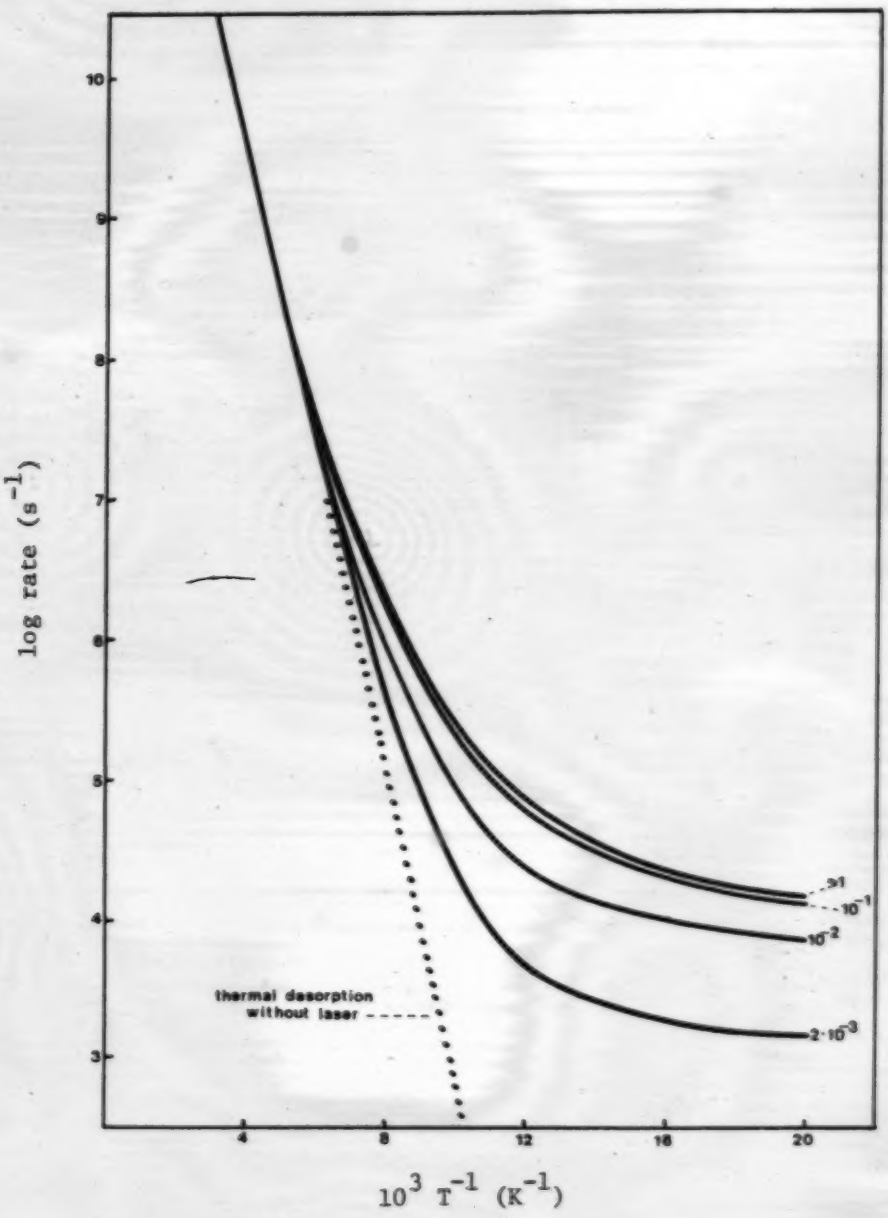

Fig. 9. Log rate versus inverse temperature for system A for different fluence values. (Fluence is in units J/m^2.)

larger than the thermal counterpart, provided the laser fluence is greater than 10^{-2} J/m^2. (See Fig. 9). At 50 K the laser enhancement is of many orders of magnitude. The fluence dependence saturates for $F_\ell \geq 1$ J/m^2. This is also seen in Fig. 8 where rate versus fluence curves level off to the right. Note that the T = 200, 250 K graphs show little fluence dependence; thermal desorption dominates in this regime. (The Debye temperature of NaCl is $T_D = 281$ K.) We shall now move on to study system B, for which a more detailed analysis is desirable.

As shown in Fig. 7, system B has fewer bound states since the range of the surface potential has been lessened. As a result, the bottom three surface states are separated by greater than one Debye energy; thermal desorption alone cannot occur from the ground state. The desorption data given in Figs. 10 and 11 for this system is rather complex, so in the next seven paragraphs we investigate the fluence and temperature dependences with reference to our microscopic model.

The log rate versus inverse temperature graphs in Fig. 11 are qualitatively similar to those for system A, except that the high temperature rates roll off just before meeting one another on a common "thermal desorption" line. This effect will be discussed shortly.

Before embarking on the main analysis, it is instructive to modify the rate equations temporarily by deleting all bound surface state transitions $j \to j'$; that is, $P^{vv'}_{jj'} = 0$. The resultingly small desorption rates are graphed as dashed lines in Fig. 11. In this very restricted case, the only desorption path is via $(j,v) = (0,0) \to (0,1) \to (0,2) \to (c,0)$. The last step in the path, $(0,2) \to (c,0)$, is the rate determining step for fluence in the range $F_\ell \geq 10^{-3}$ J/m^2. The transition rate for this step, which is $Q^{02}_{c0} + P^{02}_{c0}$, turns out to be only slightly temperature

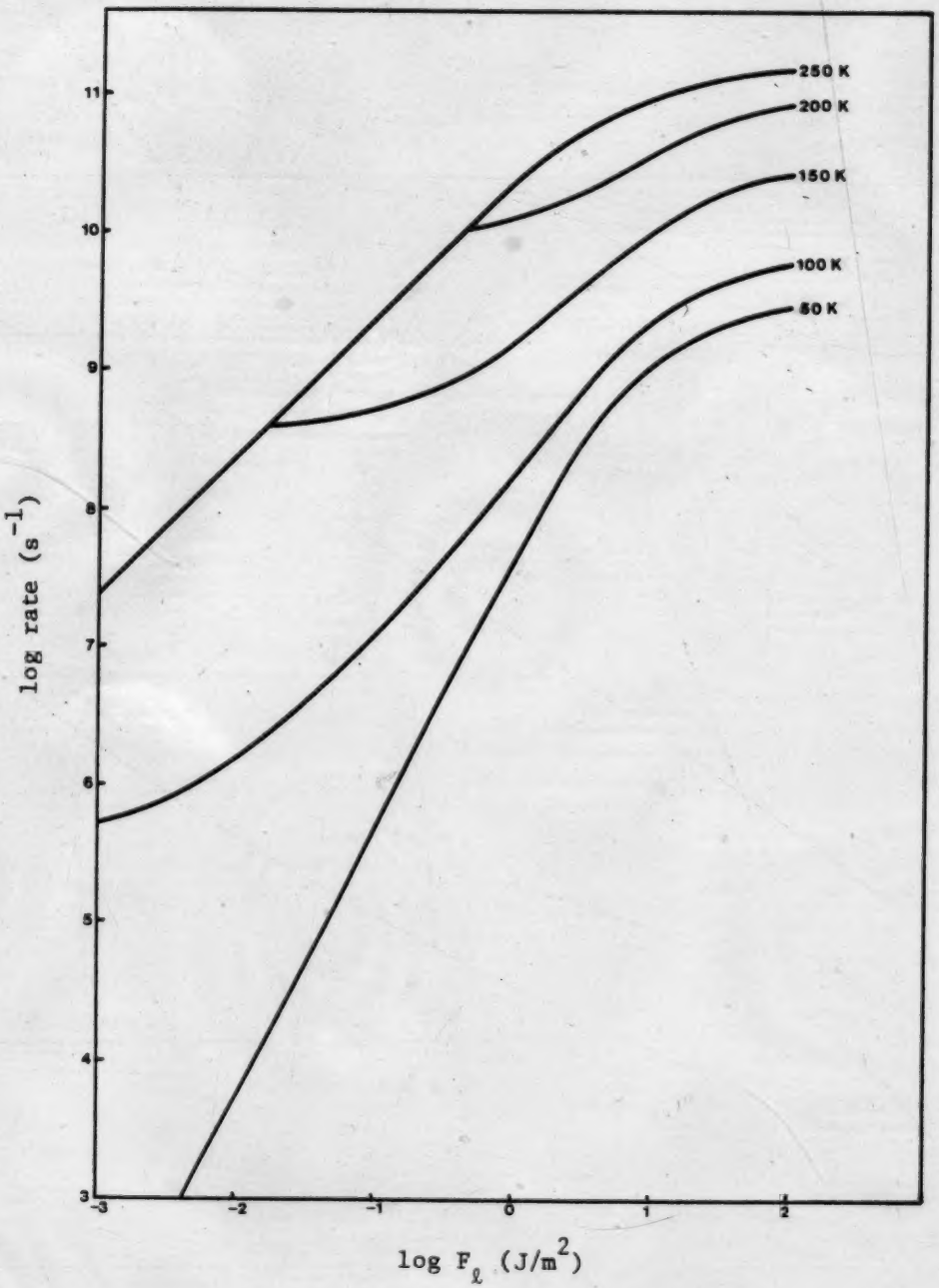

Fig. 10. Log rate versus log fluence for system B at various temperatures.

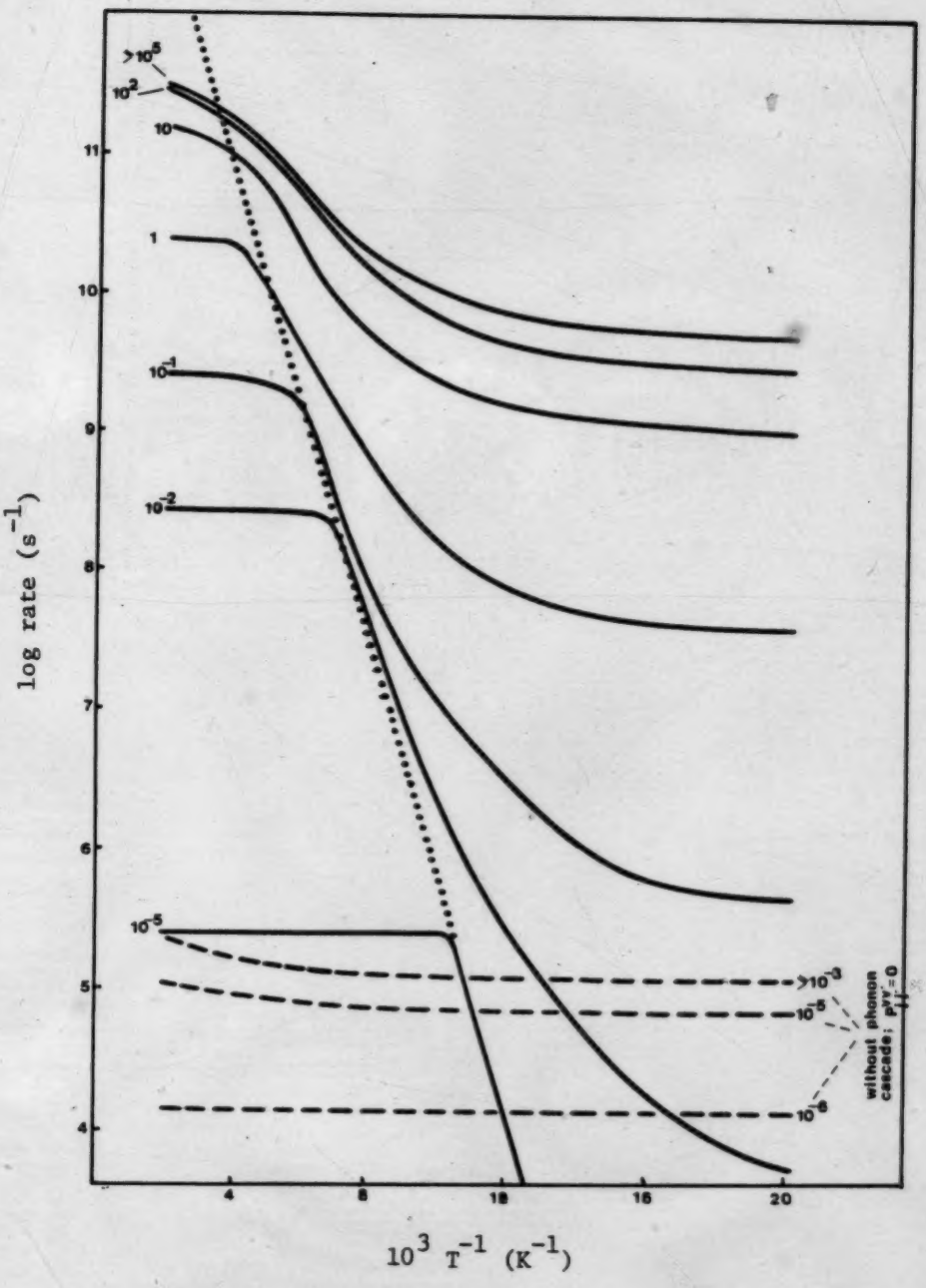

Fig. 11. Log rate versus inverse temperature for system B at different fluences. (Units of fluence are J/m^2.)

dependent. This is because Q_{c0}^{02} is temperature independent, while the phonon density of states in P_{c0}^{02} depends on temperature; see equations (87)-(89). The transition rate from (0,2) to (c,0) is thus independent of temperature at low T, but increases slightly as the Debye temperature is approached. The corresponding desorption rates shown in Fig. 11 have just this form for fluences $F_\ell \geq 10^{-3}$ J/m^2. However, for much smaller fluence the step from (0,v) to (0,v+1) is slower and becomes rate determining. For example, at $F_\ell = 10^{-6}$ J/m^2, the desorption rate in Fig. 11 is $\approx 10^{-4}$ s^{-1} at all temperatures. This is equal to the v=0 to v=1 transition rate L_{jj}^{10}. We shall now turn our attention back to the full system of rate equations.

With $P_{jj'}^{vv'}$ included, much more complex behaviour is observed in Fig. 11. To assist in our understanding of the underlying processes, we display the numerical values of just a few typical transition rates in Fig. 12. The vertical steps at the right side of this diagram correspond to the desorption path outlined in the last paragraph. It is clear from Fig. 11 that this path does not normally contribute significantly to desorption since the full-system rates are mostly much greater than those (dashed lines) predicted from this single path alone.

From Fig. 12 it is evident that vibrationally excited molecules can transfer - via a phonon interaction - to excited surface states by, for example, (j,v) = (0,1) → (5,0). The molecule can then step up and down among the surface states very rapidly with phonon assisted transition rates $P_{jj'}^{vv'}$. This "thermal cascade" is included at the left side of Fig. 12. If the molecule energy (ε_j^v) is positive, desorption may occur by a transition to the continuum. (See the top of Fig. 12). The transition rates into the continuum from a highly excited bound state -

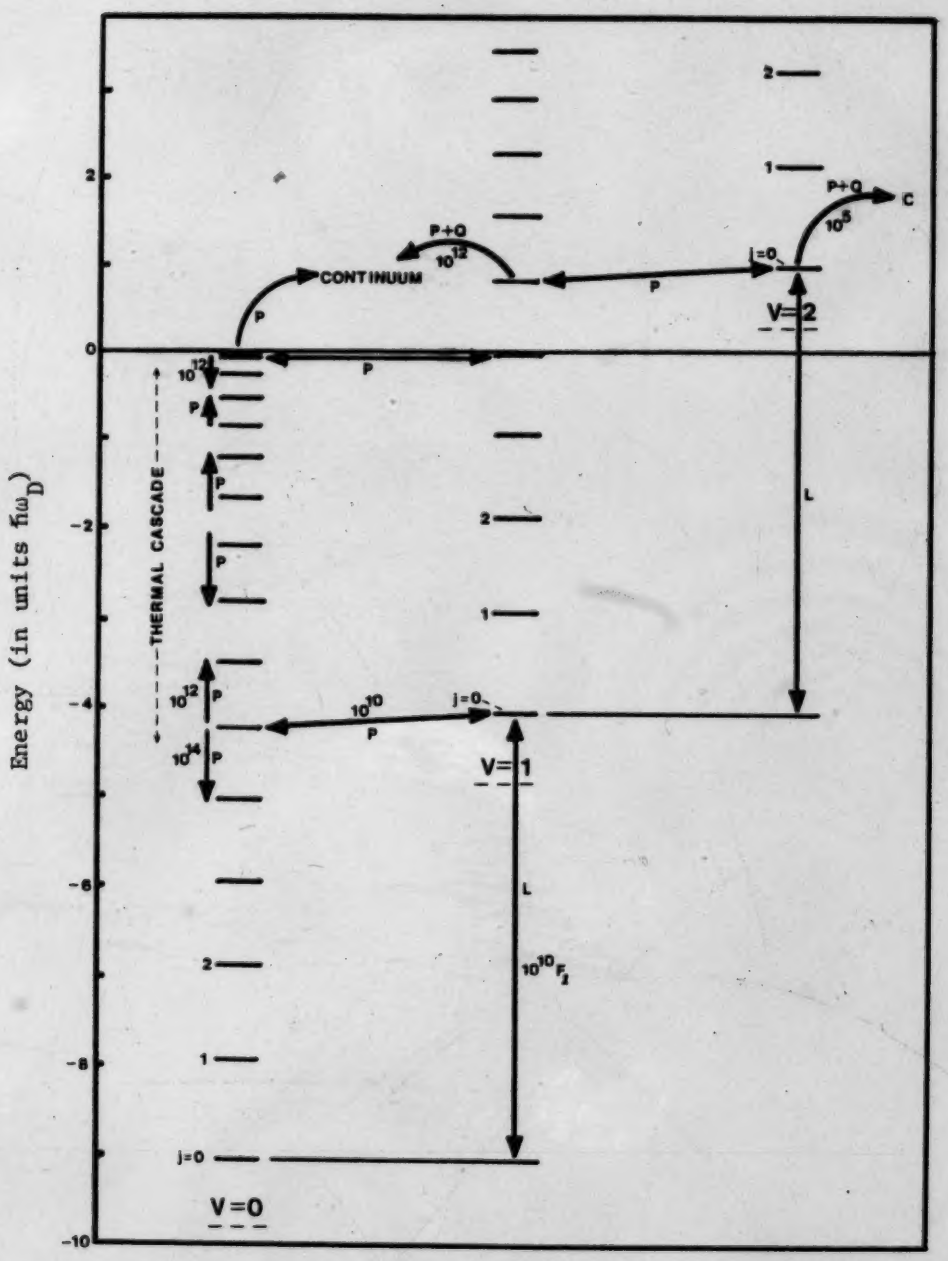

Fig. 12. Typical transitions occurring in system B. The columns of bound states (j) correspond to vibrational levels v = 0,1,2. (Rates are given for T = 50 K, in units s^{-1}.)

$j = 15$, $v = 0$ or even $j = 5$, $v = 1$ for example - are much faster than from the surface ground state, $j = 0$, $v = 2$. This is because the rates $P_{cj}^{v'v}$ and $Q_{cj}^{v'v}$ favour transitions between close surface states and adjacent vibrational states, as explained in Section 2. The actual desorption rate is determined by a complex process of competition between the complete set of transition rates. We now return to examine the photodesorption graphs in detail.

The high temperature behaviour shown in Fig. 10 is discussed first. While the low temperature graphs of rate versus fluence are qualitatively similar to those for system A, the desorption rate at $T \geq 150$ K and low fluence is limited by a straight diagonal line. This effect is a characteristic of our model, and is easily explained using Fig. 12. We begin with the adsorbate molecule in the ground state $j = 0$, $v = 0$. (For temperatures $\lesssim 150$ K the initial Boltzmann energy distribution dictates that practically all adsorbate molecules start out in the ground state.) Since the lowest surface states are separated by greater than one Debye energy, our one phonon transitions are cut off. The molecule must therefore undergo a vibrational (laser induced) transition to the $j = 0$, $v = 1$ state before proceeding further on a path to desorption. At low enough fluences, this becomes the sole rate determining step, governed by $L_{00}^{10} \simeq 10^{10} F_{\ell}$. The diagonal line in Fig. 10 obeys this equation. This effect is manifested in Fig. 11 by the rolling off of the rates at high temperatures. The roll-off points fall on a straight line (dotted line in Fig. 11) that may be characterized by an activation energy of $6.9\ \hbar\omega_D$. This is very nearly the depth of the $j = 2$ surface state, which is the lowest state accessible via one phonon processes. The dotted line appears to represent

thermal desorption from the $j = 2$ state! With this observation, we postulate that the roll-off occurs when the vibrational transiton rate, L^{10}_{jj}, is exceeded by the thermal desorption rate from the $j = 2$ state. At high temperatures, the main path to desorption apparently involves three general steps, as shown in Fig. 13. The molecule is first vibrationally excited, then couples, via phonon emission, to an excited surface state, and finally desorbs via a thermal cascade of phonon-assisted steps. The roll-off in Fig. 11, and hence the corresponding diagonal line in Fig. 10, is thus merely a result of restricting our theory to one-phonon interactions, while the lowest surface states are spaced by greater than one Debye energy.

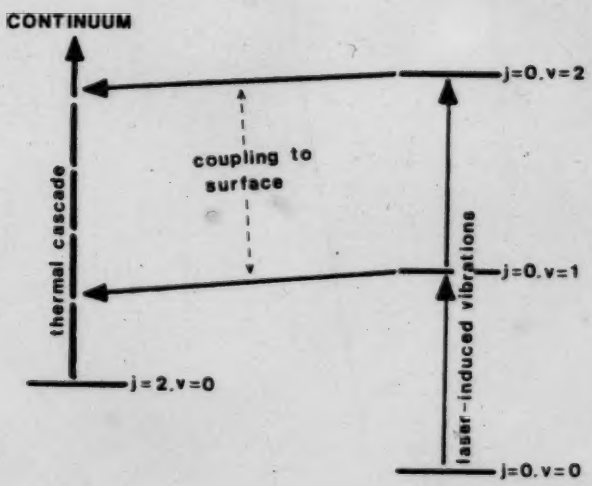

Fig. 13. Path to desorption at high temperatures for system B.

At lower temperatures now, Fig. 11 shows a very strong enhancement of desorption rate as fluence is increased. At lower fluence levels, the enhancement is less. In fact, at fluences of 10^{-2} J/m^2 and less, the photodesorption rate at T $\lesssim$ 75 K drops below that level estimated several paragraphs back by ignoring $P^{vv'}_{jj'}$! (The solid lines in Fig. 11 fall beneath dashed lines for $F_\ell \leq 10^{-2}$ J/m^2.) It appears that, at these low temperatures, the thermal cascade (see left side of Fig. 12) is directed strongly downwards because spontaneous emission of phonons dominates in the rates $P^{vv}_{jj'}$. The cascade then acts as a sink for adsorbate molecules, resulting in decreased desorption rates at low T. It appears that the temperature dependence of the desorption rates may be attributed mainly to the characteristics of the thermal cascade.

Finally, at the lowest temperature - T= 50K - the graphs in Fig.11 have mostly levelled out, to become independent of temperature. This is expected, since the individual transition rates gain their temperature dependence via the phonon density of states, which vanishes at low temperatures. The different levels for different fluences at T = 50 K indicates that the sink mechanism competes less efficiently against the desorption processes at higher fluences. While we hope that the simple interpretation given above will provide some qualitative insight into the underlying rate mechanisms involved, it is emphasized that the actual prediction of desorption rates necessitates the numerical solution of the complete master equation. This completes the analysis of system B.

The photodesorption rate graphs for system C are shown in Figs. 14 and 15. Since the bound surface states of this system are very widely spaced (see Fig. 7), the thermal cascade is expected to play a minimal

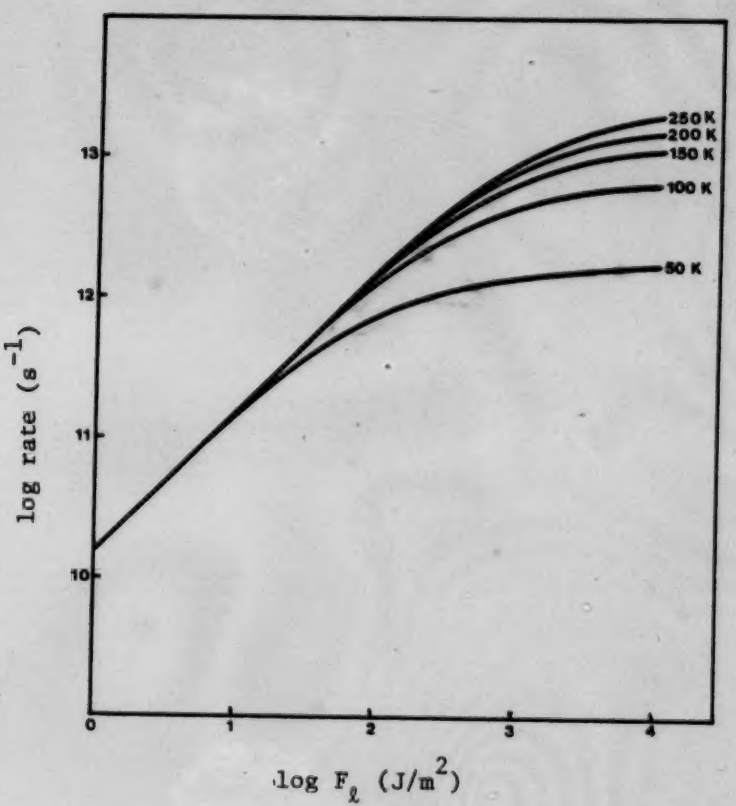

Fig. 14. Log rate versus log fluence for system C at various temperatures.

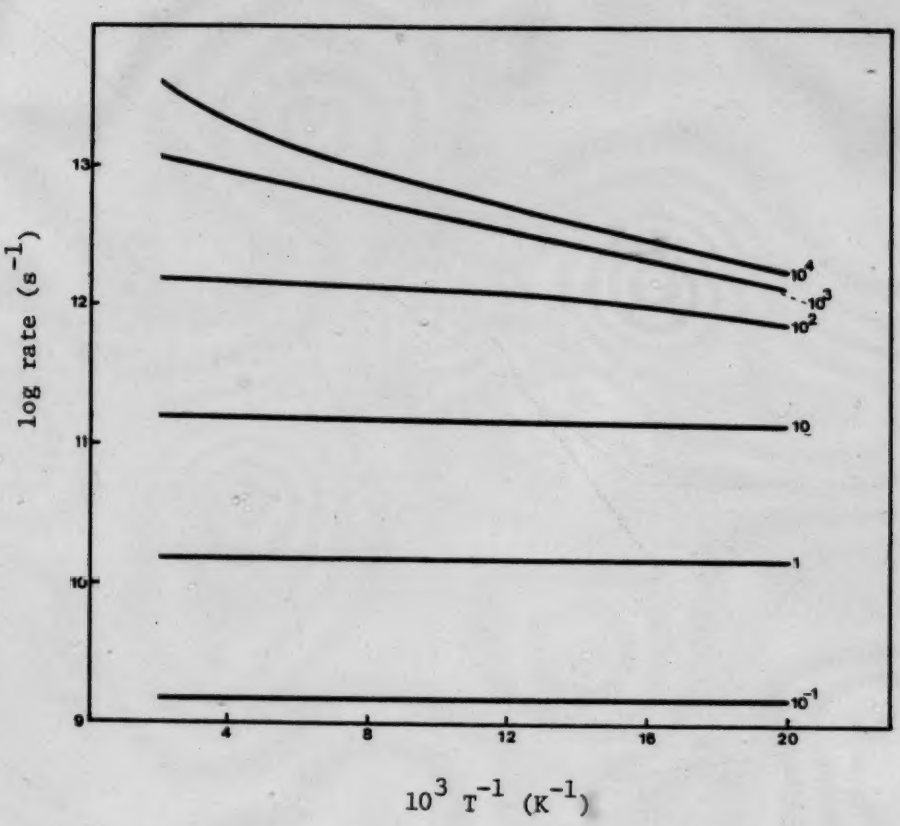

Fig. 15. Log rate versus inverse temperature for system C at various fluences. (Units of fluence are J/m^2.)

role. As a result, the temperature dependence of the photodesorption rates is considerably less than for the previous two systems.

Comparing the three systems yields important qualitative trends. As γ^{-1} is decreased (from system A to B to C), the desorption rate saturates at higher levels and at higher fluence values. The temperature dependence decreases as γ^{-1} decreases. The number of bound states also decreases with γ^{-1}, eventually preventing thermal desorption from the ground state. It is thus observed that, by varying γ^{-1} among these three systems, the characteristic fluence and temperature dependence of desorption is dramatically altered.

Equally importantly, the magnitude of the desorption rate is changed by many orders of magnitude by varying γ^{-1}. In Table 2 the

Table 2. Desorption rates (s^{-1}) at typical temperatures and fluences for the CH_3F/NaCl systems A, B, and C.

		System (γ^{-1} in Å)		
T(K)	$F_\ell(J/m^2)$	A(.35)	B(.25)	C(.15)
50	.1	1.4×10^{4}	4.5×10^{5}	1.5×10^{9}
50	100	1.5×10^{4}	2.9×10^{9}	7.6×10^{11}
150	.1	1.6×10^{7}	5.0×10^{8}	1.5×10^{9}
150	100	1.8×10^{7}	2.6×10^{10}	1.4×10^{12}
250	.1	5.2×10^{9}	2.5×10^{9}	1.5×10^{9}

desorption rate for each system is compared at several values of fluence and temperature. The rate at $F_\ell = .1$ J/m^2 and T = 50 K decreases by 5 orders as γ^{-1} is increased through systems C, B, and A. If we increase γ^{-1} further to 1 Å (then $\sigma_o = 65.2$; r = 440), the fluence dependence disappears and photodesorption is no longer detectable above the thermal rate, even at T = 50 K. This is understood to result from the fact that the rates $P^{vv'}_{jj'}$, $P^{vv'}_{cj'}$, and $Q^{vv'}_{cj'}$, become very small, exceedingly quickly, as the difference between the states - $|j-j'|$ - increases. This effect is amplified as σ_o increases with γ^{-1}. As a result, the rates $P^{vv}_{j\pm1,j}$ dominate, inducing step by step transitions in the thermal desorption cascade.

The correct choice for γ is thus crucial in modelling real systems. Additional spectroscopic data, such as bound state separation energies, may be used to fix γ more accurately.

We note, in conclusion, that our theory depends strongly on the shape and depth of the surface potential. (While the adsorbate molecular mass (m) and the Debye temperature (T_D) of the solid are also important in determining σ_o and r, these parameters are more accurately known. It will be seen - through examples in the next section - that the size of the fundamental internal molecular vibrational energy ($\hbar\omega_v$) in comparison with the well depth (V_o) is also important. On the other hand, the other characteristics of the solid and the adsorbate enter the rate equations in a much more innocuous manner.

§3.2 Comparison with Early Experimental Results; Discussion

We will now compare the theoretical data of the last section with experimental results. Although photodesorption experiments are - like

the theories - in the earliest stages, the kinetics of the CH_3F-on-NaCl system has been studied by Heidberg et al.[7]. He begins with an adsorbate of monolayer to multilayer coverage on the NaCl surface, at 64 K in a high vacuum. The sample is exposed to pulsed radiation from a high power TEA CO_2 laser which has been tuned to the vibrational frequency of the $F-CH_3$ bond. Desorbing molecules are detected with a mass spectrometer. After repeated pulses, the adsorbate coverage is depleted. At a pulse fluence of the order of $F_\ell \approx 2 \cdot 10^3$ J/m^2 - this is equivalent to an intensity of 1 MW/cm^2 - he measures the photodesorption rate $t_d^{-1} \approx 10^6$ s^{-1}, with the fluence dependence given by $t_d^{-1} \propto F_\ell^{\approx 3}$.

Our model does not immediately predict these results. A comparison with the T = 50 K line in Figs. 8, 10, and 14 shows that our model predicts too large rates for smaller systems, and much too little fluence dependence for the larger two systems which are in saturation. The maximum fluence dependence observed anywhere in our systems occurs in system B at T = 50 K, for $F_\ell \gtrsim 1$ J/m^2, where we find $t_d^{-1} \propto F_\ell^{1.9}$.

Noting that a 10% increase in V_o shifts the j = 0, v = 2 state below the continuum, we have tested the effect of this change on system B. Increasing V_o to 25 kJ/mole raises σ_o to 17.1. We now take $v_{max} = 3$, and then find that the desorption rates are not altered appreciably!

The discrepancy between our predictions and the experimental results does not necessarily imply an inconsistency. Our theory is designed for low coverage (that is, sub-monolayer) systems, in which adsorbate particles do not interact among themselves. The experiments of Heidberg et al. involve a multilayer adsorbate which will likely be influenced by interactions between adsorbate molecules. The precise

effect of such adsorbate molecule-molecule interactions, and the extent to which they may contribute to the observed discrepancy are not known. Our estimate of the dipole charge separation (Q), taken from measurements on CH_3F in the gas phase as previously mentioned, is also of questionable validity. Since the fluence coordinate scales according to Q^2, an error in Q can cause a significant shift along the fluence axis in our graphs. Such a shift could, for example, take one from a region of fluence saturation to one of considerable fluence dependence. This remains an open question until the correct value of Q is known.

Another feature that we have ignored in our discussion is surface heating, which may occur in two ways. First, the surface may absorb laser radiation directly; this effect is safely neglected in an essentially lossless dielectric, such as NaCl in the infrared. Second, the surface absorbs phonons as an adsorbate molecule cascades downwards through the surface states. The sample transition path shown in Fig. 16 shows how it may be possible for a vibrationally excited molecule to transfer almost all its energy to the phonon bath. A detailed calculation of the surface heating via this type of mechanism has not yet been done.

Photodesorption experiments on somewhat different systems have been carried out by Chuang[8]. The adsorbate is an organic ring molecule, pyridine, and desorption from both metal (Ag) and dielectric (KCl) surfaces has been observed. By varying the laser frequency, they find that the photodesorption yield is peaked at a characteristic vibrational mode of the ring molecule, indicating that the laser couples resonantly to the adsorbate molecules. On the metal surface, they estimate that direct heating of the solid contributes to 30% of the desorption at a

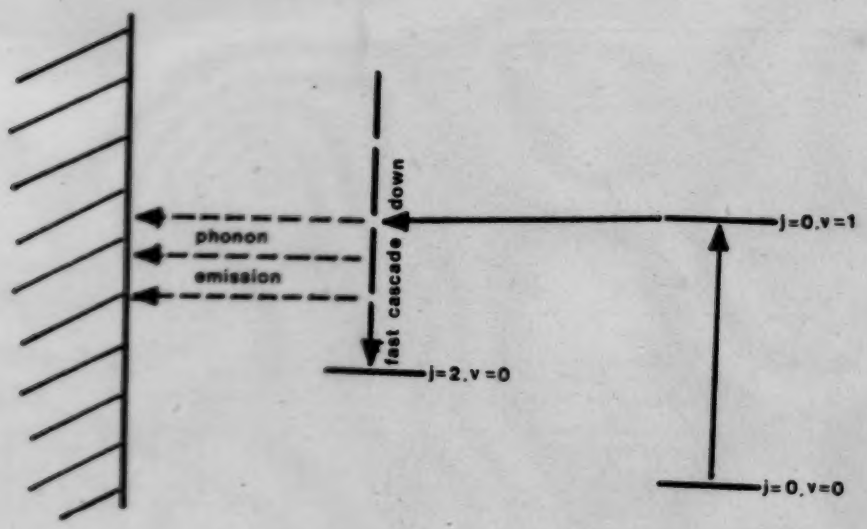

Fig. 16. A laser-induced heating mechanism for system B.

fluence $F_\ell = 10^3$ J/m^2, and to only 10% at half that fluence; the contribution drops off rapidly at lower fluences. Chuang concludes that the dominant photodesorption mechanism here must involve molecular resonant absorption of the laser radiation. We do not attempt to apply our simple (diatomic molecule) theory to the pyridine system.

Photodesorption of CO from a Cu crystal by non-resonant surface heating has been recorded by Viswanathan et al.[4] Using a high intensity laser with a pulse fluence $F_\ell \approx 10^3$ J/m^2, they desorb CO molecules at a rate $t_d^{-1} \approx 10^4$ s^{-1}. Our theory predicts that a laser with pulse fluence $F_\ell = 1$ J/m^2 tuned to the CO infrared absorption line would produce about the same desorption rate. (See Section 3.3 for details.) This prediction awaits experimental verification!

§3.3 Other Theories

It is worthwhile to compare our theory presented here with several others in the literature.

In a series of papers[5], Lin and George have developed a theory of photodesorption based on a reaction mechanism very different from ours. They suppose that the laser radiation is directly absorbed by the surface bond, and ignore coupling to the internal molecular vibrations. (This channel is shown in Fig. 1c in Section 1.) This energy absorption then induces transitions to higher energy surface states, with the assistance of the phonons of the solid. The surface bond is modelled by a harmonic potential, plus an anharmonic correction term; desorption is defined to occur when a molecule reaches a preselected energy level in this potential. Our criticism[9] of this model is two-fold:

i) Since the real surface potential is, in general, anharmonic, the associated energy level spacings will vary considerably. The laser frequency cannot be matched to all these spacings at once! The laser coupling to most of the transitions in a multi-state potential will therefore be non-resonant, and hence quite weak. (For this reason, they consider also a two laser system, with the second laser tuned to excite electronic transitions in the adsorbate too![5c]).

ii) The validity with which one may approximate the surface bond with their very simplified model potential is unclear, and apparently unnecessary, as the following authors point out.

An apparent improvement on the model described above has been made by Jedrzejek et al.[6] They consider the same desorption channel as Lin

and George, but use a much more realistic Morse potential to model the surface bond. However, this work too is subject to critizism (i) above. As a result of weak coupling to the laser radiation, Jedrzejek finds that his theory needs laser intensities four orders of magnitude larger than realistic values, to give measurable desorption yields. In contrast, our theory predicts desorption rates that saturate with respect to intensity at relatively small fluences. The predictions of our theory may be compared with Jedrzejek's in Fig. 17, where data applied to the CO-on-Cu system is graphed. Since our theory predicts much faster rates at lower fluences, it is concluded that resonant laser coupling to molecular vibrations, as employed in our theory, initiates a much more efficient photodesorption process.

Photodesorption rates have also been calculated by Lucas and Ewing[10], employing a part of the channel used in our theory. They only include the tunneling term - essentially Q_{c0}^{01} - between excited vibrational states and continuum surface states; see Fig. 18. For the system they consider (Al_2O_3), the vibrational energy spacing is much greater than the surface well depth (i.e. heat of adsorption). They assume saturation of the vibrational states, and their estimate of the desorption rate is, in their approximations, equivalent to

$$t_d^{-1} = Q_{c0}^{01} \quad . \tag{97}$$

In the specific regime they consider, our theory reduces to approximately this result too. This simple result can be easily understood after noting that transitions between excited vibrational states and bound states are highly unlikely because of the very large energy difference. Consequently, desorption proceeds mainly by the two parallel processes:

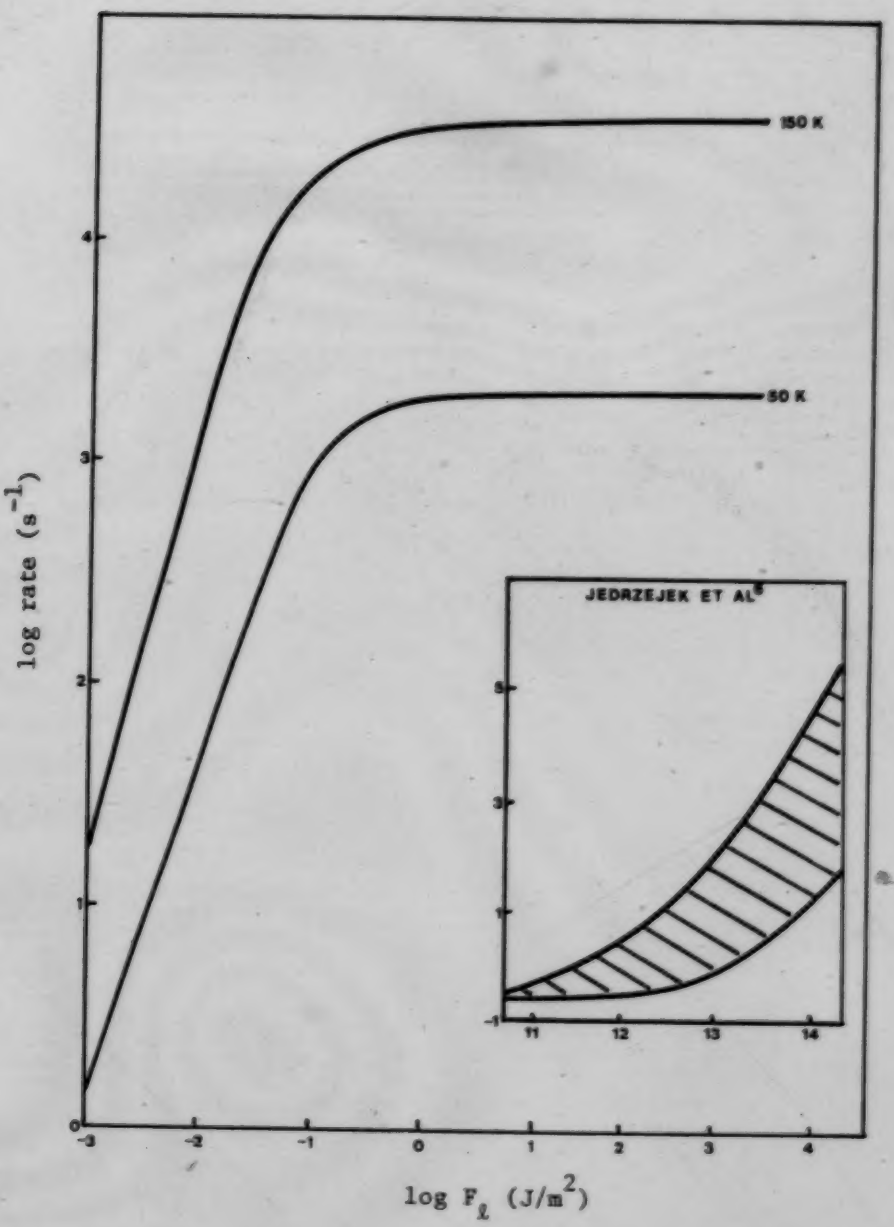

Fig. 17. Log rate versus log fluence for the CO/Cu system.

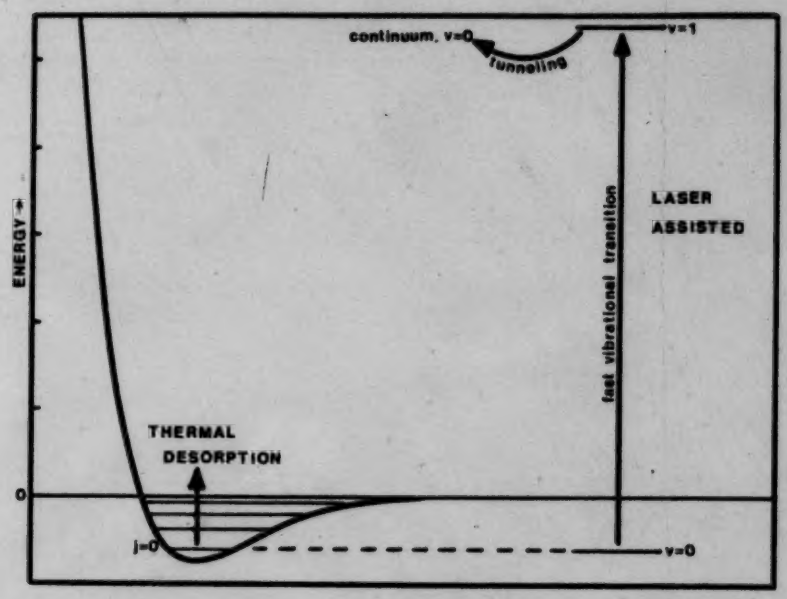

Fig. 18. Desorption mechanism for the H_2/Al_2O_3 system.

i) thermal desorption, and

ii) laser assisted via $(j,v) = (0,0) \rightarrow (0,1) \rightarrow (c,0)$.

This is illustrated in Fig. 18. At the low temperatures considered, (40 K) thermal desorption is negligible, so process (ii) dominates. For high enough laser fluence, the vibrational transitions are very fast, and hence the final jump to the continuum is the single rate-determining step. In our theory, the rate of this transition is just $Q_{c0}^{01} + P_{c0}^{01}$. Normally, $P_{c0}^{01} \lesssim Q_{c0}^{01}$; and we thus get almost the same result as (97).

Finally, we note that the authors Kreuzer and Lowy[9] have previously considered, instead of the Q_{c0}^{01} term, the effect of the P_{c0}^{01} term. This work, which involved some calculational simplifications, is in fact the beginning out of which the theory presented here has evolved.

§4. CONCLUSIONS

A fully quantum mechanical theory of desorption via laser-stimulated, resonant excitation of adsorbate molecular vibration has been presented. The theory is based on a simple microscopic model in which desorption entails a cascade of surface and vibrational state transitions. All physical parameters introduced in our model may in principle be fixed by experiments; desorption times are predicted over a full range of temperature and fluence. A comparison with other theoretical calculations and experimental results indicates that the resonant laser coupling process considered here may be a useful way to selectively and efficiently stimulate desorption. In the cases cited in Section 3, the use of a laser to excite internal molecular states appears to be much more practical than exciting the surface states directly.

An actual verification of the present theories awaits additional experiments; obtaining accurate desorption measurements is clearly not an easy task. Our theory relies on experimentally determined parameters, such as T_D, V_o, ω_v, F_ℓ, Q, and γ; the last two of these are not presently available for most systems. To check our theory, future photodesorption experiments should be performed at measured, submonolayer coverage. The potential range parameter (γ) may be determined either spectroscopically or by thermal desorption experiments done at the same coverage. (The latter method provides an evaluation of V_o too.) The molecular dipole separation (Q) may in principle be found by measurement of the infrared absorption intensities of the adsorbate. An unequivocal, experimental evaluation of our theory for resonant

photodesorption could then be obtained.

Several necessary improvements to our theory are immediately apparent. Most notable is our neglect of the surface heating effect due to phonon emission from inelastic transition processes. The seriousness of this omission should be determined by future calculations. Another weakness is our use of a one dimensional surface potential and a fixed molecular orientation. A complete three dimensional calculation (permitting molecular rotation) seems appropriate here. It must also be remembered that our theory is designed for localized, physisorbed (weakly coupled) systems at negligible surface coverage. In practice, the coverage is usually greater, allowing for significant interaction between adsorbate molecules. Resonant "V-V" coupling between molecular vibrational states in the adsorbate, as suggested by Heidberg[7c] for the CH_3F/NaCl system, is an important feature that has been ignored in the work presented here. Furthermore, we have treated the solid as a continuum throughout, and coupled the macroscopic electric field of the laser to the molecular vibrations of the adsorbate via its infrared absorption spectrum. The currently developing topic of "Surface Enhanced Raman Spectra",[22] although ignored here, may provide additional features to be utilized in future photodesorption processes on metal surfaces. There are clearly many areas open to study, both theoretical and experimental.

It summarizes to say that the utility of photodesorption - via resonant laser-molecular coupling - as a tool for selective desorption awaits the developments of many ongoing investigations.

REFERENCES

1. Z.W. Gortel, H.J. Kreuzer, and R. Teshima, Phys. Rev. B 22, 5655 (1980). (References to a series of earlier papers are given here.)

2. H.J. Kreuzer, Physica 106A, 144 (1981).

3. A review of desorption phenomena is given by D. Menzel, in R. Gomer, ed., Topics in Applied Physics, Vol. 4, Springer-Verlag, New York, 1975.

4. For a recent example, see R. Viswanathan, D.R. Burgess, Jr., P.C. Stair, and E. Weitz, J. Vac. Sci. Technol. 20(3), 605 (1982).

5. a) J.T. Lin and T.F. George, J. Chem. Phys. 66(1), 5 (1979).
   b) J.T. Lin and T.F. George, J. Chem. Phys. 72(4), 2554 (1980).
   c) J.T. Lin and T.F. George, Surf. Sci. 107, 417 (1981).

6. C. Jedrzejek, K.F. Freed, S. Efrima, and H. Metiu, Surf. Sci. 109, 191 (1981).

7. a) J. Heidberg, H. Stein, E. Riehl, and A. Nestmann, Z.F. Physikal, Chemie Neue Folge 121, 145 (1980).
   b) J. Heidberg, H. Stein, and E. Riehl, Phys. Rev. Letts. 49(9), 666 (1982).
   c) J. Heidberg, H. Stein, and E. Riehl, in Proceed. Intern. Topic. Conf. Vibrations at Surfaces, Namur (Belgium) 1980, Plenum Press, New York, 1982.

8. a) T.J. Chuang, J. Chem. Phys. 76(7), 3828 (1982).
   b) T.J. Chuang and H. Seki, Phys. Rev. Letters 49(6), 382 (1982).

9. H.J. Kreuzer and D.N. Lowy, Chem. Phys. Lett. 78(1), 50 (1981).

10. D. Lucas and G.E. Ewing, Chem. Phys. 58, 385 (1981).

11. J.D. Jackson, Classical Electrodynamics, 2nd ed., John Wiley & Sons, New York, 1975, pp. 278-82.

12. H. Haken, Quantum Field Theory of Solids, North-Holland, Amsterdam, 1976, pp. 77-87.

13. W.H. Louisell, Quantum Statistical Properties of Radiation, John Wiley & Sons, New York, 1973, pp. 252-3.

14. Ref. 11, p. 574.

15. Z.W. Gortel, H.J. Kreuzer and R. Teshima, Phys. Rev. B 22, 512 (1980).

16. Ref. 13, p. 63.

17. E. Goldys, Z.W. Gortel and H.J. Kreuzer, Surf. Sci. 116, 33 (1982).

18. H. Ezawa, Ann. Phys. (NY) 67, 438 (1971).

19. Z.W. Gortel, H.J. Kreuzer and D. Spaner, J. Chem. Phys. 72(1), 234 (1980).

20. Z.W. Gortel, H.J. Kreuzer, R. Teshima and L.A. Turski, Phys. Rev. B 24(8), 4456 (1981).

21. G.M. Barrow and D.C. McKean, Proc. Royal Soc. 213A, 27 (1952).

22. For example, M. Fleishman, P.J. Hendra and A.J. McQuillan, Chem. Phys. Lett. 26, 163 (1974).
T. Lopez-Rios, C. Pettenkofer, I. Pockrand, and A. Otto, Surf. Sci. 121, L541 (1982).

23. M. Abramowitz and I.A. Stegun, Handbook of Mathematical Functions, National Bureau of Standards, Washington D.C., 1965.

APPENDIX A

Orthogonality of $\{\vec{U}_{\vec{k}\beta}\}$

Equation (14) is now derived for the modes $\vec{U}_{\vec{k}\beta}(\vec{x})$ defined in equations (13a,b). Using (13a),

$$\int d\vec{x}\, n^2(x)\vec{U}_{\vec{k}\beta}(\vec{x})\cdot\vec{U}_{\vec{k}'\beta'}(\vec{x}) = \frac{1}{4\pi^2}\int d\vec{R}\, e^{i(\vec{K}-\vec{K}')\vec{R}}\int dx\, n^2(x)\vec{f}^{\beta}_{\vec{K}\zeta}(x)\cdot\vec{f}^{\beta'*}_{\vec{K}'\zeta'}(x)$$

$$= \delta(\vec{K}-\vec{K}')\delta_{\beta\beta'}\int dx\, n^2(x)\vec{f}^{\beta}_{\vec{K}\zeta}(x)\cdot\vec{f}^{\beta*}_{\vec{K}\zeta}(\vec{x}) \qquad \text{(A1)}$$

The remaining integral in (A1) must be evaluated explicitly for the cases $\beta = s,p$. Using equation (13b) in the s-polarization case gives

$$\int_{-\infty}^{\infty} dx\, n^2(x)\vec{f}^{s}_{\vec{K}\zeta}(x)\cdot\vec{f}^{s}_{\vec{K}\zeta'}(x) = N^{s*}N^{s}\left\{\frac{2}{(1+n_r a)}\,\frac{2}{(1+n_r a')}\,n_r^2\int_{-\infty}^{0} dx\, e^{i(b'-b)x}\right.$$

$$\left. + \int_{0}^{\infty} dx\left(e^{i\zeta x}+\frac{1-n_r a}{1+n_r a}e^{-i\zeta x}\right)\left(e^{-i\zeta' x}+\frac{1-n_r a'}{1+n_r a'}e^{i\zeta' x}\right)\right\}$$

$$= N^{s*}N^{s}\,\frac{2\pi}{(1+n_r a)(1+n_r a')}\left\{(1+2n_r a+n_r^2 a^2)\,\delta(\zeta'-\zeta) + \text{a term involving}\right.$$

$$\left.\delta(\zeta'+\zeta)\right\} \qquad \text{(A2)}$$

where a' and b' are evaluated at ζ'. To arrive at the second line above, we note that

$$\int_{0}^{\infty} dx\, e^{i(\zeta'-\zeta)x} = i\,\frac{\mathcal{P}}{\zeta-\zeta'} + \pi\delta(\zeta'-\zeta)$$

where $\mathcal{P}$ denotes the principle part distribution. The terms involving $\mathcal{P}/\zeta-\zeta'$ all cancel in equation (A2). Since we require $\zeta,\zeta' < 0$, the term in (A2) proportional to $\delta(\zeta'+\zeta)$ does not contribute. With N^s defined as

$$N^s = \frac{1+n_r a}{\sqrt{2\pi(1+2n_r a+n_r^2 a^2)}} \qquad \text{(A3)}$$

equation (A2) reduces to

$$\int_{-\infty}^{\infty} dx\, n^2(x)\, \vec{f}^{s}_{\vec{K}\zeta}(x)\cdot\vec{f}^{s}_{\vec{K}\zeta'}(x) = \delta(\zeta'-\zeta) \quad . \tag{A4}$$

Similarly, substitution of (13b) into (A1) for the p-polarization case and performing analogous manipulations yields

$$\int_{-\infty}^{\infty} dx\, n^2(x)\, \vec{f}^{p}_{\vec{K}\zeta}(x)\cdot\vec{f}^{p}_{\vec{K}\zeta'}(x) = \delta(\zeta'-\zeta) \tag{A5}$$

where

$$N^{p} = \frac{n_r + a}{\sqrt{2\pi(K^2+\zeta^2)(n_r^2 + 2n_r^2 a + a^2)}} \quad . \tag{A6}$$

Finally, substituting (A4) and (A6) into (A1) gives the orthogonality relation

$$\int d\vec{x}\, n^2(x)\vec{U}_{\vec{k}\beta}(\vec{x})\vec{U}^{*}_{\vec{k}'\beta'}(\vec{x}) = \delta_{\beta\beta'}\delta(\vec{K}-\vec{K}')\delta(\zeta-\zeta') = \delta_{\beta\beta'}\delta(\vec{k}-\vec{k}') \quad . \tag{A7}$$

Equation (15) is derived in a similar manner. Using (13a), we have

$$\int d\vec{x}\, n^2(x)\vec{U}_{\vec{k}\beta}(\vec{x})\cdot\vec{U}_{\vec{k}'\beta'}(\vec{x}) = \frac{1}{4\pi^2}\int d\vec{R}\, e^{i(\vec{K}+\vec{K}')\vec{R}}\int dx\, n^2(x)\vec{f}^{\beta}_{\vec{K}\zeta}(x)\cdot\vec{f}^{\beta}_{\vec{K}'\zeta'}(x)$$

$$= \delta(\vec{K}+\vec{K}')\delta_{\beta\beta'}\int dx\, n^2(x)\vec{f}^{\beta}_{\vec{K}\zeta}(x)\cdot\vec{f}^{\beta}_{-\vec{K}\zeta'}(x) \quad . \tag{A8}$$

Evaluating the integral over x using the same method as before leads to

$$\int d\vec{x}\, n^2(x)\vec{U}_{\vec{k}\beta}(\vec{x})\cdot\vec{U}_{\vec{k}'\beta'}(\vec{x}) = -\Lambda_{\vec{k}\beta}\,\delta(\vec{K}+\vec{K}')\delta(\zeta-\zeta') \tag{A9}$$

where

$$\Lambda_{\vec{k}s} = \frac{1 - n_r^2 a^2}{1 + 2n_r a + n_r^2 a^2} \quad \text{and} \quad \Lambda_{\vec{k}p} = -\frac{n_r^2 - a^2}{n_r^2 + 2n_r a + a^2} \quad . \tag{A10}$$

APPENDIX B

The Morse Wave Functions

The eigen-solutions to the Schrödinger equation for the Morse potential,

$$-\frac{\hbar^2}{2m}\frac{d^2}{dx^2}\Phi(x)+V_o(e^{-2\gamma(x-x_o)}-2e^{-\gamma(x-x_o)})\Phi(x)=E\Phi(x) \tag{B1}$$

are quoted directly from reference 1. The energy eigenvalues take on discrete, bound state levels given by

$$E_j = -\frac{\hbar^2\gamma^2}{2m}s_j^2 \tag{B2}$$

where $s_j = \sigma_o - j - \frac{1}{2}$, $j = 0,1,\ldots j_{max} < \sigma_o - \frac{1}{2}$, $\sigma_o^2 = \frac{2mV_o}{\hbar^2\gamma^2}$.
There is a continuum of free states with energy

$$E_q = \frac{\hbar^2 q^2}{2m} \tag{B3}$$

where q is the wave vector of the particle.

The bound state wave functions are

$$\Phi_j(x) = \sqrt{\gamma}\,\phi_j(\zeta) \tag{B4}$$

where $\zeta = \gamma(x-x_o)$ and

$$\phi_j(\zeta) = (2\sigma_o)^{s_j}\,\Gamma^{-\frac{1}{2}}(2s_j)\left[\begin{matrix}2s_j+j\\ j\end{matrix}\right]^{-\frac{1}{2}}\exp(-\sigma_o e^{-\zeta})\exp(-s_j\zeta)L_j^{2s_j}(2\sigma_o e^{-\zeta}) \tag{B5}$$

in terms of the Laguerre polynomial $L_j^{2s_j}(u)$.

The continuum state wavefunctions, normalized in a box of length L, are given by

$$\Phi_q(x) = L^{-\frac{1}{2}}\,\phi_\eta(\zeta)$$

where $\eta = q/\gamma$ and

$$\phi_\eta(\zeta) = \left|\frac{(\frac{1}{2}-\sigma_o-i\eta)}{(2i\eta)}\right| \exp(-\sigma_o e^{-\zeta})\, e^{-i\eta\zeta}\,\psi(\tfrac{1}{2}-\sigma_o+i\eta, 1+2i\eta, 2\sigma_o e^{-\zeta}) \tag{B7}$$

with the confluent hypergeometric function $\Psi(a,b,z)$ defined as

$$\Psi\left(\frac{1}{2}-\sigma_o+i\eta,1+2i\eta,z\right)=\frac{i\pi}{\sinh(2\pi\eta)}\left\{\frac{F(\frac{1}{2}-\sigma_o+i\eta,1+2i\eta,z)}{\Gamma(1+2i\eta)\Gamma(\frac{1}{2}-\sigma_o-i\eta)}-\right.$$

$$\left.-\,z^{-2i\eta}\,\frac{F(\frac{1}{2}-\sigma_o-i\eta,1-2i\eta,z)}{\Gamma(1-2i\eta)\Gamma(\frac{1}{2}-\sigma_o+i\eta)}\right\}\quad . \tag{B8}$$

$F(z,b,z)$ is a Kummer's function, as defined in reference 23.

APPENDIX C

Evaluation of the Integral $I_{\ell jj'}$

The integral $I_{\ell jj'}$ may be rewritten by substituting the wave functions (B5) into (76b) to get

$$I_{\ell jj'} = \frac{1}{2\sigma_o}\sqrt{\frac{j!j'!2s_j 2s_{j'}}{\Gamma(2s_j+j+1)\Gamma(2s_{j'}+j'+1)}}\sum_{\ell jj'}^{\zeta_o} \tag{C1}$$

where

$$\sum_{\ell jj'}^{\zeta_o} = \int_0^{2\sigma_o e^{\zeta_o}} du\, e^{-u} u^{s_j+s_{j'}} \left(\frac{2^\ell}{2\sigma_o}u - 1\right) L_j^{2s_j}(u) L_j^{2s_{j'}}(u) \simeq \sum_{\ell jj'}^{\infty} \tag{C2}$$

(We have substituted $u = 2\sigma_o e^{-\xi}$.)

The method of evaluation of $\sum_{\ell jj'}^{\infty}$ described below follows that used by R. Teshima to do similar integral in reference 1. We first separate (C2) into two parts

$$\sum_{\ell jj'}^{\infty} = \frac{2^\ell}{2\sigma_o} I_1 - I_o \tag{C3}$$

where

$$I_i = \int_0^{\infty} du\, e^{-u} u^{(2\sigma_o - j - j' - 1 + i)} L_j^{2\sigma_o - 2j - 1}(u)\, L_{j'}^{2\sigma_o - 2j' - 1}(u) . \tag{C4}$$

Since I_o is symmetric with respect to j,j', we let $j > j'$. We then expand $L_j^{2\sigma_o - 2j - 1}(u)$ using

$$L_n^{\alpha}(x) = \frac{e^x x^{-\alpha}}{n!}\frac{d^n}{dx^n}\left(e^{-x} x^{n+\alpha}\right) \tag{C5}$$

and then integrate I_o by parts j times to get

$$I_o = (-1)^{j+j'} \frac{\Gamma(2\sigma_o - j)}{j'!} . \tag{C6}$$

Similar operations performed on I_1 lead to

$$I_1 = (-1)^{j+j'} \frac{\Gamma(2\sigma_o - j)}{j'!}\left[(j+1)(2\sigma_o - j) - j'(2\sigma_o - j' - 1)\right]. \tag{C7}$$

Now, substitution of (C6) and (C7) into equation (C4) gives

$$\sum_{\ell jj'}^{\infty} = (-1)^{j+j'} \frac{j-j'}{j'!} \Gamma(2\sigma_o - j)\, 2^{\ell} \left[1 - \frac{j+j'+1}{2\sigma_o} + \frac{1-2^{-\ell}}{j-j'}\right]. \qquad \text{(C8)}$$

We finally get $I_{\ell jj'}$ by substitution into equation (C1).

The corresponding integral including bound and continuum state wave functions ($I_{\ell qj'}$) is almost identical to one appearing in reference 1, so we just quote the final result here:

$$I_{\ell\eta j'} = (-1)^{j'} 2^{\ell} (2\sigma_o)^{-2-i\eta} \sqrt{\frac{(2\sigma_o - 2j'-1)}{j'!\Gamma(2\sigma_o - j')}} \frac{|\Gamma(\tfrac{1}{2}-\sigma_o - i\eta)|}{|\Gamma(2i\eta)|}$$

$$\times |\Gamma(\sigma_o + \tfrac{1}{2} + i\eta)|^2 [(\sigma_o - j' - \tfrac{1}{2})^2 + \eta^2 + 2\sigma_o(1 - 2^{-\ell})] \qquad \text{(C9)}$$

where $\eta = q/\gamma$.